Dynamic localization of the chromosomal passenger complex is controlled by the orphan kinesins KIN-A and KIN-B in the kinetoplastid parasite *Trypanosoma brucei*

Daniel Ballmer[1] and Bungo Akiyoshi[1,2,*]

[1]Department of Biochemistry, University of Oxford, South Parks Road, Oxford, OX1 3QU, United Kingdom

[2]The Wellcome Centre for Cell Biology, Institute of Cell Biology, School of Biological Sciences, Edinburgh, EH9 3BF, United Kingdom

[*]Correspondence to bungo.akiyoshi@ed.ac.uk

Abstract

The chromosomal passenger complex (CPC) is an important regulator of cell division, which shows dynamic subcellular localization throughout mitosis, including kinetochores and the spindle midzone. In traditional model eukaryotes such as yeasts and humans, the CPC consists of the catalytic subunit Aurora B kinase, its activator INCENP, and the localization module proteins Borealin and Survivin. Intriguingly, Aurora B and INCENP as well as their localization pattern are conserved in kinetoplastids, an evolutionarily divergent group of eukaryotes that possess a unique set of kinetochore proteins and lack homologs of Borealin or Survivin. It is not understood how the kinetoplastid CPC assembles or how it is targeted to its subcellular destinations during the cell cycle. Here, we identify two orphan kinesins, KIN-A and KIN-B, as bona fide CPC proteins in *Trypanosoma brucei*, the causative agent of African sleeping sickness. By employing biochemical, structural, and cell biological approaches, we demonstrate that KIN-A and KIN-B serve as the scaffold for the assembly of the remaining CPC subunits. Kinetochore localization of the CPC depends on the KKT7 – KKT8 complex pathway, with the C-terminal unstructured tail of KIN-A serving as a key interaction partner for the KKT8 complex. Our data therefore show that, unlike other eukaryotes that take advantage of histone modifications for centromere recruitment, trypanosomes rely on kinetochore proteins to recruit the CPC onto kinetochores. Furthermore, the ATPase activity of KIN-A promotes chromosome alignment in prometaphase and CPC translocation to the central spindle upon anaphase onset. Thus, KIN-A constitutes a unique 'two-in-one' CPC localization module in complex with KIN-B, which directs the CPC to kinetochores (from S phase until metaphase) via its C-terminal tail, and to the central spindle (in anaphase) via its N-terminal kinesin motor domain. Our findings

34 highlight the evolutionary diversity of CPC proteins and raise the possibility that kinesins may have
35 served as the original transport vehicles for Aurora B kinases in early eukaryotes.
36

37 ## Introduction

38 During cell division, duplicated genetic material must be distributed equally into two daughter cells.
39 The Aurora B kinase is a key mitotic regulator widely conserved among eukaryotes (Hochegger et al.,
40 2012). It undergoes dynamic localization changes throughout mitosis to enable the spatially
41 restricted phosphorylation of substrates involved in chromosome alignment, chromosome bi-
42 orientation, spindle assembly checkpoint (SAC) signalling, and cytokinesis (Carmena et al., 2012). In
43 early mitosis, Aurora B is first detected on chromosome arms and during prometaphase becomes
44 enriched at centromeres, where it destabilizes incorrect kinetochore-microtubule attachments
45 (Krenn and Musacchio, 2015). Upon anaphase onset, Aurora B translocates to the spindle midzone,
46 and during cytokinesis associates with the equatorial cortex to regulate cell abscission (Adams et al.,
47 2000; Cooke et al., 1987; Trivedi and Stukenberg, 2016).
48 The dynamic localization pattern of the Aurora B kinase is in part achieved through its
49 association with a scaffold comprised of inner centromere protein (INCENP), Borealin and Survivin
50 (Adams et al., 2001, 2000; Gassmann et al., 2004; Romano et al., 2003; Sampath et al., 2004; Vader
51 et al., 2006; Wheatley et al., 2001). Together, these proteins form a tetrameric complex referred to
52 as the chromosomal passenger complex (CPC). The CPC can be partitioned into two functional
53 modules: The 'catalytic module' and the 'localization module'. The catalytic module is composed of
54 Aurora B in complex with the IN-box at the INCENP C-terminus, which is required for full activation
55 of the Aurora B kinase (Bishop and Schumacher, 2002). The localization module comprises Borealin,
56 Survivin and the N-terminus of INCENP, which are connected to one another via a three-helical
57 bundle (Jeyaprakash et al., 2011, 2007; Klein et al., 2006). The two modules are linked by the central
58 region of INCENP, composed of an intrinsically disordered domain and a single alpha helical (SAH)
59 domain. INCENP harbors microtubule-binding domains within the N-terminus and the central SAH
60 domain, which play key roles for CPC localization and function (Cormier et al., 2013; Fink et al., 2017;
61 Kang et al., 2001; Mackay et al., 1993; Nakajima et al., 2011; Noujaim et al., 2014; Samejima et al.,
62 2015; van der Horst et al., 2015; Wheatley et al., 2001; Wheelock et al., 2017).
63 In vertebrates, recruitment of the CPC to centromeric chromatin depends on two pathways,
64 involving the Haspin and Bub1 kinases. Haspin phosphorylates histone H3 on Thr3 (H3T3ph), which is
65 recognized by the baculovirus IAP repeat (BIR) domain of Survivin (Kelly et al., 2010; Wang et al.,
66 2010; Yamagishi et al., 2010). H3T3ph is initially found along the entire length of chromosomes
67 between sister chromatids but becomes enriched at the inner centromere (the space between sister

68 kinetochores) during late prophase. In contrast, the kinetochore-associated Bub1 kinase
69 phosphorylates histone H2A on Thr120 (H2AT120ph) (Kawashima et al., 2010). H2AT120ph recruits
70 Shugoshin-like proteins (Sgo1 and Sgo2), which in turn are bound by Borealin (Tsukahara et al., 2010;
71 Yamagishi et al., 2010). Recently, Sgo1 has also been demonstrated to interact with the BIR domain
72 of Survivin through an N-terminal histone H3-like motif (Abad et al., 2022; Jeyaprakash et al., 2011).
73 The interactions of Borealin and Survivin with Sgo1 form the basis for a kinetochore-proximal pool of
74 the CPC which is distinct from the inner centromere pool (Broad et al., 2020; Hadders et al., 2020;
75 Liang et al., 2020).

76 In most studied eukaryotes, ranging from yeast to humans, kinetochore assembly is
77 scaffolded by a centromere-specific histone H3 variant, CENP-A (Allshire and Karpen, 2008; Black and
78 Cleveland, 2011; Hori and Fukagawa, 2012; Maddox et al., 2012; Westhorpe and Straight, 2013). An
79 assembly of inner kinetochore protein complexes, referred to as the constitutive centromere-
80 associated network (CCAN), interacts with centromeric CENP-A chromatin throughout the cell cycle
81 and provides a platform for recruitment of the outer kinetochore KNL1/Mis12 complex/Ndc80
82 complex (KMN) network that has microtubule-binding activity (Cheeseman et al., 2006; Foltz et al.,
83 2006; Izuta et al., 2006; Okada et al., 2006). Some of these kinetochore proteins are present in
84 nearly all sequenced eukaryotes, suggesting that key principles of chromosome segregation are
85 widely shared among eukaryotes (Drinnenberg and Akiyoshi, 2017; Van Hooff et al., 2017; Meraldi et
86 al., 2006; Tromer et al., 2019). However, a unique set of kinetochore proteins (KKT1–20, KKT22–25,
87 KKIP1–12) are present in the evolutionarily divergent lineage called kinetoplastids (Akiyoshi, 2020;
88 Akiyoshi and Gull, 2014; D'Archivio and Wickstead, 2017; Nerusheva et al., 2019; Nerusheva and
89 Akiyoshi, 2016). Kinetoplastids are flagellated protists that are highly divergent from commonly
90 studied eukaryotes (Cavalier-Smith, 2010). *Trypanosoma brucei*, *Trypanosoma cruzi*, and *Leishmania*
91 spp. are causative agents of African trypanosomiasis, Chagas disease, and leishmaniasis,
92 respectively, and as such pose a serious threat to public health and prosperity across the tropics and
93 subtropics (Stuart et al., 2008; WHO, 2017).

94 Despite the absence of canonical kinetochore components (Berriman et al., 2005; Lowell and
95 Cross, 2004), Aurora kinases are conserved in kinetoplastids. Early studies suggested that the Aurora
96 B homolog (Aurora B^{AUK1}) in *T. brucei* forms a complex with chromosomal passenger complex
97 proteins 1 and 2 (CPC1 and CPC2) and plays a crucial role in mitosis and cytokinesis (Li et al., 2008;
98 Tu et al., 2006). CPC1 was later found to be a divergent INCENP homolog (hereafter referred to as
99 $INCENP^{CPC1}$) based on the presence of a conserved C-terminal IN-box (Hu et al., 2014). However,
100 $INCENP^{CPC1}$ lacks the central SAH domain and N-terminal residues, which in other eukaryotes interact
101 with Survivin and Borealin. In addition, two orphan kinesins, KIN-A and KIN-B, have been proposed

102 to transiently associate with Aurora B^{AUK1} during mitosis (Li, 2012; Li et al., 2008). Although homologs
103 of the 'localization module' proteins Survivin and Borealin have not been identified in kinetoplastids
104 (Komaki et al., 2022), the trypanosome CPC displays a dynamic localization pattern similar to that of
105 the metazoan CPC (Li et al., 2008): Aurora B^{AUK1}, INCENP^{CPC1} and CPC2 localize to kinetochores in
106 early mitosis and then translocate to the central spindle upon anaphase onset. From late anaphase
107 onwards, an additional population of CPC proteins is detectable at the tip of the new flagellum
108 attachment zone (FAZ), the point of cytokinesis initiation in *T. brucei*. It is presently not understood
109 how the CPC assembles in these evolutionarily divergent eukaryotes nor how its localization
110 dynamics are regulated during the cell cycle.

111 Here, by combining biochemical, structural and cell biological approaches in procyclic form
112 *T. brucei*, we show that the trypanosome CPC is a pentameric complex comprising Aurora B^{AUK1},
113 INCENP^{CPC1}, CPC2, and the two orphan kinesins KIN-A and KIN-B. KIN-A and KIN-B interact via their
114 coiled-coil domains to form a subcomplex within the CPC, which serves as a scaffold for the catalytic
115 module (Aurora B^{AUK1} + INCENP^{CPC1}). The C-terminal unstructured tail of KIN-A directs kinetochore
116 localization of the CPC from S phase to metaphase, while the N-terminal motor domain promotes
117 the central spindle enrichment in anaphase. Furthermore, we identify the KKT7 – KKT8 complex
118 pathway as the main kinetochore recruitment arm of the trypanosome CPC.

119

120 Results

121

122 KIN-A and KIN-B are bona fide CPC proteins in trypanosomes

123 To identify additional interactors of the CPC in trypanosomes, we performed immunoprecipitation
124 followed by liquid chromatography tandem mass spectrometry (IP-MS) of endogenously YFP-tagged
125 Aurora B^{AUK1} (Fig. S1A, Table S1 and Table S2). Besides Aurora B^{AUK1}, INCENP^{CPC1} and CPC2, we
126 observed notable enrichment of two orphan kinesins, KIN-A and KIN-B (Wickstead and Gull, 2006),
127 as reported previously (Li et al., 2008). Both KIN-A and KIN-B were also highly enriched in
128 immunoprecipitates of ectopically expressed GFP-INCENP^{CPC1}. Vice versa, IP-MS of GFP-tagged KIN-A
129 and KIN-B identified Aurora B^{AUK1}, INCENP^{CPC1}, and CPC2 as top hits (Fig. 1A and Table S2).

130 We next assessed the localization dynamics of fluorescently tagged KIN-A and KIN-B over the
131 course of the cell cycle (Figs. 1, B-E). *T. brucei* possesses two DNA-containing organelles, the nucleus
132 ('N') and the kinetoplast ('K'). The kinetoplast is an organelle found uniquely in kinetoplastids, which
133 contains the mitochondrial DNA and replicates and segregates prior to nuclear division. The 'KN'
134 configuration serves as a good cell cycle marker (Siegel et al., 2008; Woodward and Gull, 1990). To
135 our surprise, KIN-A-YFP and GFP-KIN-B exhibited a CPC-like localization pattern similar to that of

136 Aurora B^{AUK1}: Both kinesins localized to kinetochores from S phase to metaphase, and then
137 translocated to the central spindle in anaphase (Figs. 1, C-E). Moreover, like Aurora B^{AUK1}, a
138 population of KIN-A and KIN-B localized at the new FAZ tip from late anaphase onwards (Figs. S1, B
139 and C). This was unexpected, because KIN-A and KIN-B were previously reported to localize to the
140 spindle but not to kinetochores or the new FAZ tip (Li et al., 2008). These data suggest that KIN-A
141 and KIN-B are bona fide CPC proteins in trypanosomes, associating with Aurora B^{AUK1}, INCENP^{CPC1},
142 and CPC2 throughout the cell cycle.

143 A bioinformatic search for homologs of CPC proteins within Euglenozoa revealed that both
144 KIN-A and KIN-B are present in trypanosomatids and bodonids, with KIN-A homologs detectable
145 even in prokinetoplastids (Fig. 1F) (Materials and Methods). CPC2, on the other hand, was
146 detectable only within trypanosomatids. Aurora B^{AUK1} and INCENP^{CPC1} are present in kinetoplastids as
147 well as in diplonemids and euglenids (sister groups of kinetoplastids). Interestingly, homologs of
148 Borealin, Survivin, KIN-A, or KIN-B were not detectable in diplonemids or euglenids, raising a
149 possibility that these organisms may also possess 'non-canonical' CPC proteins. We conclude that
150 the KIN-A and KIN-B kinesins are highly conserved within kinetoplastids, constituting integral
151 components of the CPC in this evolutionary divergent group of eukaryotes.

152

153 **KIN-A and KIN-B promote kinetochore localization of the CPC**

154 To investigate which subunits of the CPC are responsible for its kinetochore targeting, we performed
155 a series of RNAi experiments (Figs. 2, A-E). Because CPC2 is poorly conserved among kinetoplastids
156 (Fig. 1F) and depletion of CPC2 using two different hairpin RNAi constructs (Table S1) was inefficient,
157 we did not include CPC2 in these experiments. As previously reported (Li et al., 2008), depletion of
158 Aurora B^{AUK1}, INCENP^{CPC1}, KIN-A or KIN-B resulted in a prominent growth defect (Fig. S2A) with cells
159 arresting in G2/M (2K1N) (Fig. S2B). Knockdown of Aurora B^{AUK1} did not affect the kinetochore
160 localization of YFP-tagged INCENP^{CPC1}, KIN-A or KIN-B (Figs. 2, A and C-E). Knockdown of INCENP^{CPC1}
161 caused delocalization of Aurora B^{AUK1} but not of KIN-A or KIN-B (Figs. 2, A and B, D and E). In contrast,
162 both Aurora B^{AUK1} and INCENP^{CPC1} were delocalized upon depletion of KIN-A or KIN-B (Figs. 2, A-C).
163 RNAi against KIN-A disrupted KIN-B localization and vice versa (Figs. 2, A, D and E). Moreover, total
164 protein levels of KIN-B were affected by depletion of KIN-A (Fig. S2C), suggesting that the interaction
165 with KIN-A is required to stabilize KIN-B.

166 We next ectopically expressed GFP-tagged truncations of KIN-A and KIN-B to assess which
167 domains promote their kinetochore targeting. Both KIN-A and KIN-B contain an N-terminal kinesin
168 motor domain followed by several predicted coiled-coil motifs (Li et al., 2008), although KIN-B is
169 predicted to be an inactive motor (Wickstead and Gull, 2006). In addition, KIN-A has a long C-

170 terminal tail. Unlike full-length KIN-B, KIN-B$^{2-316}$ (inactive motor domain) failed to enrich at
171 kinetochores and was instead found in the nucleolus (Fig. S2, D and E). KIN-A$^{2-309}$ (motor domain)
172 was also primarily detected in the nucleolus, although we observed additional spindle and weak
173 kinetochore-like signal in some metaphase cells (Fig. 2G). By contrast, both KIN-A$^{310-862}$ (coiled-coil
174 domain + C-terminal disordered tail) and KIN-B$^{317-624}$ (coiled-coil domain) clearly localized to
175 kinetochores from S phase to metaphase (Fig. 2H; Fig. S2F). Intriguingly, unlike endogenously YFP-
176 tagged KIN-A, ectopically expressed GFP fusions of both full-length KIN-A and KIN-A$^{310-862}$ localized at
177 kinetochores even in anaphase (Figs. 2, F and H). Weak anaphase kinetochore signal was also
178 detectable for KIN-B$^{317-624}$ (Fig. S2F). GFP fusions of the central coiled-coil domain or the C-terminal
179 disordered tail of KIN-A did not localize to kinetochores (data not shown). These results show that
180 kinetochore localization of the CPC is mediated by KIN-A and KIN-B and requires both the central
181 coiled-coil domain as well as the C-terminal disordered tail of KIN-A.
182
183 **Structural model of the trypanosome CPC**
184 To gain structural insights into the trypanosome CPC, we used AlphaFold2 (AF2) (Jumper et al., 2021;
185 Mirdita et al., 2022) to predict the overall structure of the trypanosome CPC by testing combinations
186 of full-length Aurora B^{AUK1}, INCENP^{CPC1}, CPC2, KIN-A, and KIN-B, and truncations thereof (Figs. S3, A-
187 D). AF2 confidently predicted parallel coiled coils between KIN-A and KIN-B, with the main region of
188 interaction contained within the central region of KIN-A (residues ~310–550) and the C-terminal
189 region of KIN-B (residues ~320–580). The C-terminal tail (residues ~550–862) of KIN-A is predicted to
190 be intrinsically disordered (pLDDT scores <20, Figs. S3, A and B). The first ~55 residues of INCENP^{CPC1},
191 predicted to form two α-helices (residues ~7–20 and ~36–55), interact with the coiled coils of KIN-
192 A:KIN-B in close proximity to the kinesin motors. A flexible central linker in INCENP^{CPC1} bridges the N-
193 terminus of INCENP^{CPC1} and the catalytic module of the CPC (Aurora B^{AUK1} + INCENP^{CPC1} IN-box).
194 Similarly to INCENP^{CPC1}, an N-terminal α-helical region in CPC2 (residues ~19–75) interacts with the
195 KIN-A:KIN-B coiled coils immediately downstream of the INCENP^{CPC1} binding site. Consistent with
196 these predictions, GFP-tagged INCENP$^{CPC1\ 2-147}$ or CPC2$^{2-120}$ displayed normal localization dynamics
197 indistinguishable from the corresponding full-length constructs (Figs. S3, E-F and H-I). In contrast,
198 deletion of the N-terminal domains of INCENP^{CPC1} or CPC2 impaired kinetochore localization (Figs.
199 S3, G and J). Together, these data suggest that Aurora B^{AUK1} forms a subcomplex with the C-terminus
200 of INCENP^{CPC1}, and that INCENP^{CPC1} and CPC2 interact with the coiled-coil domain of KIN-A:KIN-B via
201 their N-terminal domains.
202 To validate these findings biochemically, we performed bis(sulfosuccinimidyl) suberate (BS^3)
203 cross-linking of native CPC complexes isolated by immunoprecipitation of endogenously tagged YFP-

204 Aurora B^{AUK1} from cells arrested prior to anaphase, followed by mass spectrometry analysis (IP-
205 CLMS) (Fig. 3A and Table S2). Indeed, our IP-CLMS data revealed high-score crosslinks between the
206 predicted coiled-coil domains of KIN-A and KIN-B, suggesting that the two kinesins form a parallel
207 heterodimer. As expected, Aurora B^{AUK1} formed contacts with the C-terminal IN-box of INCENP^{CPC1},
208 consistent with these two proteins constituting the catalytic module of the CPC. The N-terminal
209 region of INCENP^{CPC1} interacted mainly with KIN-B and to a lesser degree with KIN-A, with most
210 contacts confined to the N-terminal ends of the predicted coiled-coil domains of the kinesins close
211 to their motor domains. The N-terminus of CPC2, on the other hand, formed crosslinks with the
212 coiled-coil domain of KIN-A. We used PyXLinkViewer (Schiffrin et al., 2020) to map our IP-CLMS data
213 onto the assembled AF2 model of the trypanosome CPC (Fig. 3B). Using a Euclidian distance cut-off
214 of 30 Å, ~85% of crosslinks were compatible with the model, providing confidence in the AF2
215 predictions. The few crosslinks that violated the distance constraints mainly represent intra-protein
216 contacts between the INCENP^{CPC1} N- and C-terminal domains or inter-protein contacts between the
217 INCENP^{CPC1} C-terminal domain and the kinesin motor domain of KIN-A. The central domain of
218 INCENP^{CPC1} is predicted to be unstructured (pLDDT scores <20, Figs. S3, C-D) and may act as a flexible
219 linker, permitting multiple orientations of the catalytic module relative to the KIN-A:KIN-B scaffold.
220 Taken together, these data indicate that KIN-A and KIN-B interact via their coiled-coil domains,
221 which serve as a scaffold for the assembly of the remaining CPC subunits.
222
223 **The CPC is recruited to kinetochores through the KKT7 – KKT8 complex pathway**
224 Core components of the Haspin-H3T3ph and Bub1-H2AT120ph-Sgo1 pathways that control CPC
225 recruitment to the centromere in other model eukaryotes are not found in kinetoplastids (Berriman,
226 2005), and so far, no centromere-specific histone modifications and/or histone variants have been
227 uncovered in *T. brucei*. We reasoned that the centromere receptor(s) of the trypanosome CPC may
228 lie within the repertoire of unconventional kinetochore proteins present in kinetoplastids. Our IP-
229 CLMS approach failed to detect crosslinks between CPC subunits and kinetochore components
230 (Table S2), possibly due to the transient nature of these interactions. Nevertheless, several KKT
231 proteins were commonly enriched in the immunoprecipitates of Aurora B^{AUK1}, CPC1, KIN-A and KIN-
232 B, the most abundant ones being KKT6, KKT7, KKT8, KKT9, KKT10, KKT11 and KKT12 (Fig. 1A; Fig. S1A
233 and Table S2). KKT7 is detected at kinetochores from S phase until the end of anaphase and recruits
234 the KKT8 complex (comprising KKT8, KKT9, KKT11 and KKT12) (Akiyoshi and Gull, 2014; Ishii and
235 Akiyoshi, 2020). The KKT8 complex localizes at kinetochores from S phase and dissociates at the
236 metaphase-anaphase transition.

237 Using previously validated RNAi constructs (Akiyoshi and Gull, 2014; Llauró et al., 2018;
238 Marcianò et al., 2021), we found that knockdown of KKT7 or KKT9 resulted in dispersal of YFP-Aurora
239 B^{AUK1} from kinetochores in ~70% of cells (Figs. 4, A-D). In contrast, depletion of KKT1, KKT2, KKT3,
240 KKT4, KKT6, KKT10/19, KKT14 and KKT16 had little or no effect on YFP-Aurora B^{AUK1} localization (Figs.
241 S4, A and B). KIN-A-YFP was also lost from kinetochores upon RNAi-mediated depletion of KKT8
242 complex subunits (Figs. S4, C and D). We next tested whether KKT7 or the KKT8 complex were able
243 to recruit Aurora B^{AUK1} to an ectopic locus using the LacI-LacO system (Landeira and Navarro, 2007).
244 For these experiments, we expressed GFP tagged $KKT7^{2-261}$ or KKT8 fused to the Lac repressor (LacI)
245 in trypanosomes containing an ectopic Lac operator (LacO) array stably integrated into rDNA
246 repeats. We previously showed that KKT7 lies upstream of the KKT8 complex (Ishii and Akiyoshi,
247 2020). Indeed, GFP-$KKT7^{2-261}$-LacI recruited tdTomato-KKT8, -KKT9 and -KKT12 (Fig. S4E). Expression
248 of GFP-$KKT7^{2-261}$-LacI or GFP-KKT8-LacI resulted in robust recruitment of tdTomato-Aurora B^{AUK1} to
249 LacO foci in S phase (Figs. 4, E and F). Intriguingly, we also noticed that, unlike endogenous KKT8
250 (which is not present in anaphase), ectopically expressed GFP-KKT8-LacI remained at kinetochores
251 during anaphase (Fig. 4F). This resulted in a fraction of tdTomato-Aurora B^{AUK1} being trapped at
252 kinetochores during anaphase instead of migrating to the central spindle (Fig. 4F). We observed a
253 comparable situation upon ectopic expression of GFP-KIN-A, which is retained on anaphase
254 kinetochores together with tdTomato-KKT8 (Fig. S4F). In contrast, Aurora B^{AUK1} was not recruited to
255 LacO foci marked by GFP-$KKT7^{2-261}$-LacI in anaphase (Fig. 4E).
256
257 **KKT7 recruits the KKT8 complex via the KKT9:KKT11 subcomplex**
258 To gain further insights into the structure and assembly hierarchy within the KKT7 – KKT8 complex
259 pathway, we performed CLMS on native complexes isolated by immunoprecipitation of
260 endogenously YFP-tagged kinetochore proteins and mapped the detected crosslinks onto AF2
261 structure prections (Figs. 4, G and H) (Materials & Methods). AF2 confidently predicted coiled coils
262 between KKT8 and KKT12 and between KKT9 and KKT11 (Fig. 4G; Figs. S4, G and H), suggesting that
263 KKT8:KKT12 and KKT9:KKT11 each form distinct subcomplexes. To validate these findings, we co-
264 expressed combinations of 6HIS-KKT8, KKT9, KKT11, and KKT12 in *E. coli* and performed metal
265 affinity chromatography (Fig. 4I). 6HIS-KKT8 efficiently pulled down KKT9, KKT11, and KKT12, as
266 shown previously (Ishii and Akiyoshi, 2020). In the absence of KKT9, 6HIS-KKT8 still pulled down
267 KKT11 and KKT12. Removal of either KKT9 or KKT11 did not impact formation of the KKT8:KKT12
268 subcomplex. In contrast, 6HIS-KKT8 could not be recovered without KKT12, indicating that KKT12 is
269 required for formation of the full KKT8 complex. These results support the idea that the KKT8
270 complex consists of KKT8:KKT12 and KKT9:KKT11 subcomplexes. The two subcomplexes appear to be

271 connected to each other through interactions between the C-terminal region of the KKT8:KKT12
272 coiled coils and the C-terminus of KKT11. Two alpha helices in KKT7$^{2-261}$ (residues ~149–181) are
273 predicted to interact with KKT9:KKT11. Using a distance cut-off of 30 Å, ~70% of crosslinks were
274 compatible with the model (Figs. 4, G and H). Of the crosslinks that failed to meet the distance
275 criteria, ~90% involved unstructured regions within KKT7 or the C-terminal tail of KKT8. Collectively,
276 our results reveal that KKT7 recruits the KKT8 complex through interaction with the KKT9:KKT11
277 subcomplex.
278 We next examined the localization dependency of KKT8 complex components in cells. Using
279 RNAi constructs against individual subunits of the KKT8 complex (Akiyoshi and Gull, 2014; Ishii and
280 Akiyoshi, 2020; Marcianò et al., 2021), we assessed localization of endogenously YFP-tagged KKT8,
281 KKT9 and KKT12 (Figs. S4, I-L). We found that knockdown of any subunit of the KKT8 complex
282 affected protein levels and kinetochore localization of the other subunits, indicating that presence of
283 all subunits is required to stabilize the full complex. YFP-KKT9 was least affected and was still
284 detectable at kinetochores in ~50% of cells depleted of KKT8, KKT11 or KKT12 (Fig. S4L). Thus,
285 KKT9:KKT11 may lie upstream of KKT8:KKT12. Indeed our IP-CLMS data suggest that the KKT9:KKT11
286 subcomplex directly interacts with the N-terminus of KKT7 (Fig. 4H, Table S2). KKT7 also formed
287 robust crosslinks with the KKT10/19 kinases (Table S2), supporting our previous finding that KKT7
288 and KKT10 form a stable complex (Ishii and Akiyoshi, 2020). Together, these data suggest that the
289 KKT7 – KKT8 complex pathway serves as the main CPC recruitment arm in trypanosomes.
290
291 **The KIN-A C-terminal tail interacts with the KKT8 complex through a conserved domain**
292 By IP-CLMS we failed to detect reliable crosslinks between the CPC and the KKT7 – KKT8 complex or,
293 in fact, any kinetochore proteins (Table S2). This suggests that the IP-CLMS approach, although well-
294 suited for characterizing stable protein complexes, may not be sensitive enough to detect transient
295 or lower affinity interactions. To overcome this, we used AF2 to probe for potential interactions
296 between the KKT8 complex and CPC (sub)complex. AF2 did not predict interactions between the
297 KKT8 complex and INCENP^{CPC1}, CPC2 or KIN-B (data not shown). Intriguingly, AF2 predicted with high
298 confidence interactions between KKT9:KKT11 and a conserved region (residues ~722–741) within the
299 KIN-A C-terminal tail, which we termed conserved domain 1 (CD1) (Figs. 5, A and B; Figs. S5, A and
300 B). This interaction involves a triple helix composed of KIN-A CD1, KKT9, and KKT11 in a region close
301 to the KKT7-binding site. pLDDT scores improved significantly for KIN-A CD1 in complex with
302 KKT9:KKT11 (>80) compared to KIN-A CD1 alone (~20) (Fig. S3, A and B), suggesting that CD1 forms a
303 helical structure upon binding to KKT9:KKT11. Sequence alignment revealed the presence of a
304 second conserved domain (residues ~816–862) within the C-terminal tail of KIN-A, hereafter referred

305 to as CD2 (Fig. 5B; Fig. S5A). To assess the contributions of CD1 and CD2 for kinetochore recruitment
306 of KIN-A in vivo, we ectopically expressed GFP fusions of the central coiled coils and C-terminal tail of
307 KIN-A (residues ~310–862) lacking either CD1, CD2, or both (Figs. S5, C-F). GFP-KIN-A$^{310\text{-}862\ \Delta CD2}$
308 showed a moderate reduction in kinetochore localization in metaphase and was completely lost
309 from kinetochores in anaphase (Figs. S5, D and G). By contrast, GFP-KIN-A$^{310\text{-}862\ \Delta CD1}$ was largely
310 dispersed in metaphase but reappeared at kinetochores in anaphase (Figs. S5, E and G). GFP-KIN-
311 A$^{310\text{-}716}$ lacking both CD1 and CD2 failed to enrich at kinetochores both in metaphase and anaphase
312 (Figs. S5, F and G). These data suggest that CD1 and CD2 synergistically promote kinetochore
313 localization of KIN-A, with CD1 interacting with KKT9:KKT11 and CD2 possibly interacting with
314 another receptor at the kinetochore.
315 We next tested the relevance of KIN-A CD1 and CD2 for CPC localization and function by
316 replacing one allele of KIN-A with C-terminally tagged wild-type or mutant constructs lacking either
317 CD1 or CD2 and performed RNAi against the 3'UTR of KIN-A to deplete the untagged allele. We were
318 unable to obtain a rescue cell line lacking both CD1 and CD2 as the double-mutant protein was not
319 properly expressed. Wild-type KIN-A-YFP along with Aurora B^{AUK1} robustly localized to kinetochores
320 from S phase until anaphase onset (Figs. 1, C and D; Fig. 5C). KIN-A$^{\Delta CD1}$-YFP was detectable at
321 kinetochores in G2 but predominantly localized to the mitotic spindle from (pro)metaphase onwards
322 (Figs. 5, D and F), indicating that removal of CD1 severely weakens the affinity of KIN-A for
323 kinetochores and instead shifts the balance towards microtubule binding. Interestingly, expression
324 of KIN-A$^{\Delta CD1}$-YFP similarly affected the localization of Aurora B^{AUK1} (Figs. 5, D and G; Fig. S5H). We also
325 detected partial spindle localization of Aurora B^{AUK1} in a small population (~25%) of metaphase cells
326 expressing KIN-A$^{\Delta CD2}$-YFP (Figs. 5, E-G). Central spindle localization of KIN-A in anaphase was
327 unaffected by deletion of either CD1 or CD2 (Figs. 5, D and E). Remarkably, despite a substantial loss
328 of Aurora B^{AUK1} from kinetochores in metaphase, ΔCD1 cells exhibited normal cell cycle profiles (Fig.
329 S5I) and showed only a modest decrease in proliferation rates (Fig. 5H). This parallels the situation in
330 budding yeast, in which error-free chromosome segregation can be sustained even when inner
331 centromere localization of Aurora B is largely abolished (Campbell and Desai, 2013; García-Rodríguez
332 et al., 2019).
333
334 **CPC targeting to the central spindle in anaphase depends on KIN-A's ATPase activity**
335 Finally, we asked how translocation of the CPC to the spindle midzone in anaphase is achieved in
336 trypanosomes. In mammalian cells, dephosphorylation of INCENP and the kinesin MKLP2 upon
337 anaphase onset allows formation of a transient CPC-MKLP2 complex (Gruneberg et al., 2004;
338 Hümmer and Mayer, 2009; Kitagawa et al., 2014; Serena et al., 2020). MKLP2 activity then drives

339 plus-directed movement of this complex along microtubules of the anaphase spindle. We therefore
340 speculated that anaphase translocation of the kinetoplastid CPC to the central spindle may involve
341 the kinesin motor domain of KIN-A. KIN-B is unlikely to be a functional kinesin based on the absence
342 of several well-conserved residues and motifs within the motor domain, which are fully present in
343 KIN-A (Li et al., 2008). These include the P-loop, switch I and switch II motifs, which form the
344 nucleotide binding cleft, and many conserved residues within the α4-L12 elements, which interact
345 with tubulin (Fig. S6A) (Endow et al., 2010). Consistent with this, the motor domain of KIN-B,
346 contrary to KIN-A, failed to localize to the mitotic spindle when expressed ectopically (Fig. S2E) and
347 did not co-sediment with microtubules in our in vitro assay (Fig. S6B).
348 Ectopically expressed GFP-KIN-A and -KIN-A$^{2-309}$ partially localized to the mitotic spindle but
349 failed to concentrate at the midzone during anaphase (Figs. 2, F and G), suggesting that N-terminal
350 tagging of the KIN-A motor domain may interfere with its function. To address whether the ATPase
351 activity of KIN-A is required for central spindle localization of the CPC, we replaced one allele of KIN-
352 A with a C-terminally YFP-tagged G210A ATP hydrolysis-defective rigor mutant (Fig. 6A) (Rice et al.,
353 1999) and used an RNAi construct directed against the 3'UTR of KIN-A to deplete the untagged
354 allele. The rigor mutation did not affect recruitment of KIN-A to kinetochores (Figs. S6, C and D).
355 However, KIN-A^{G210A}-YFP marked kinetochores were misaligned in ~50% of cells arrested in
356 metaphase, suggesting that ATPase activity of KIN-A promotes chromosome congression to the
357 metaphase plate (Figs. S6, E-H). In anaphase, the KIN-A rigor mutant failed to concentrate at the
358 central spindle and instead widely decorated the mitotic spindle, with increased signal observed at
359 spindle poles possibly due to poleward flux (Figs. 6, B and C). Expression of the KIN-A^{G210A} rigor
360 mutant prevented Aurora B^{AUK1} from translocating to the central spindle and caused lagging
361 chromosomes (Figs. 6, D-F). The KIN-A rigor mutation also slowed cell proliferation even in the
362 presence of wild-type protein and caused accumulation of cells in anaphase (Figs. 6, G and H). We
363 conclude that central spindle localization of the CPC depends on KIN-A's ATPase activity and is
364 required for proper chromosome segregation.
365
366
367 **Discussion**
368
369 Whereas astonishing diversity in kinetochore composition is seen among eukaryotes (Hooff et al.,
370 2017; Komaki et al., 2022; Tromer et al., 2019), the proteins of the regulatory circuitry underlying
371 chromosome segregation, such as the APC/C, SAC and CPC, are more widely conserved. Homologs of
372 the CPC proteins Aurora B kinase and its associated partner INCENP have been detected in almost all

373 sequenced eukaryotes, including kinetoplastids. The dynamic localization pattern exhibited by the
374 CPC (e.g. transferring from centromeres to the central spindle upon metaphase-anaphase transition)
375 is likewise highly conserved across eukaryotes but appears to be achieved through a variety of
376 mechanisms. For instance, while CPC recruitment to the centromeres in higher eukaryotes is
377 governed by two histone phosphorylation marks (Haspin-mediated H3T3ph and Bub1-mediated
378 H2AT120ph), budding yeasts employ a combination of histone modifications (Bub1-mediated
379 H2AT121ph) and kinetochore proteins as CPC receptors. Borealin^{Bir1} not only recognizes Sgo1 but
380 also interacts with the CBF3 complex through Ndc10 (Cho and Harrison, 2011; Yoon and Carbon,
381 1999). Furthermore, INCENP^{Sli15}/Aurora B^{Ipl1} interact with the Ctf19 subunit of the COMA complex at
382 kinetochores (Fischböck-Halwachs et al., 2019). The proteins that form the localization module of
383 the CPC in different species appear to mirror the diversity in centromeric CPC receptors. In fact,
384 many phyla lack Borealin or Survivin homologs (Komaki et al., 2022). Komaki et al. recently identified
385 two functionally redundant CPC proteins in *Arabidopsis*, Borealin Related Interactor 1 and 2 (BORI1
386 and 2), which engage in a triple helix bundle with INCENP and Borealin using a conserved helical
387 domain, but employ an FHA domain instead of a BIR domain to read H3T3ph (Komaki et al., 2022).
388 In this study, we have identified KIN-A and KIN-B as components of the CPC in
389 trypanosomes, and delineated a novel pathway for centromeric recruitment of the CPC in this
390 evolutionary divergent group of eukaryotes. In agreement with our work, an early study on the CPC
391 in *T. brucei* found that KIN-A and KIN-B co-purified with Aurora B^{AUK1}, INCENP^{CPC1} and CPC2 based on
392 a pull-down of an Aurora B^{AUK1}-PTP fusion protein followed by mass spectrometry analysis (Li et al.,
393 2008). However, HA-tagged KIN-A and KIN-B were not detected at kinetochores (from late
394 interphase until metaphase) nor at the new FAZ tip (from late anaphase), and hence were not
395 interpreted as CPC proteins. Contrary to this report, our data clearly show that KIN-A and KIN-B are
396 constitutive components of the CPC in *T. brucei*. First, YFP-tagged KIN-A and KIN-B co-localize with
397 Aurora B^{AUK1}, INCENP^{CPC1} and CPC2 throughout the cell cycle. Second, KIN-A and KIN-B are readily
398 detected within native CPC complexes isolated by immunoprecipitation of CPC subunits from cells
399 arrested prior to anaphase and form robust crosslinks with the other CPC subunits. Finally, YFP-
400 Aurora B^{AUK1} and INCENP^{CPC1}-YFP are crucially dependent on KIN-A and KIN-B for localizing both to
401 metaphase kinetochores and to the anaphase central spindle. Thus, the KIN-A:KIN-B subcomplex
402 constitutes the localization module of the trypanosome CPC.
403 Biochemical, cell biological and in silico modelling approaches indicate that the kinesins KIN-
404 A and KIN-B form coiled coils between their central and C-terminal domains, respectively, which
405 then serve as a scaffold onto which INCENP^{CPC1} and CPC2 assemble via their N-terminal α-helical
406 domains. The catalytic module of the trypanosomes CPC, consisting of Aurora B^{AUK1} bound to the C-

407 terminal IN-box of INCENP^{CPC1}, is connected to the KIN-A:KIN-B scaffold through a flexible linker in
408 INCENP^{CPC1}. While our on-beads cross-linking of native CPCs suggests that the catalytic module is
409 positioned in close proximity to the kinesin heads, this may not necessarily be true in vivo. For
410 example, the catalytic module may exist in both 'locked' and 'open' conformations with regard to its
411 association with the kinesin motor domains. We speculate that the interaction of the KIN-A motor
412 domain with microtubules from prometaphase onwards may cause the catalytic module to
413 disengage from its kinesin head-associated state (Fig. 7). In analogy to the SAH domain of INCENP in
414 other model eukaryotes which has been proposed to function as a dog leash (Samejima et al., 2015;
415 Santaguida and Musacchio, 2009), the INCENP^{CPC1} flexible linker in trypanosomes (~100 amino acids
416 long) may then permit Aurora B^{AUK1} to roam across a larger but nevertheless spatially constrained
417 target area to phosphorylate its substrates while still being anchored to the kinetochore via KIN-
418 A:KIN-B. Importantly, this mechanism would allow the CPC to act as an intrinsic 'sensor' of KT-MT
419 attachments. Such models dealing with alternative conformations of the CPC in various cellular
420 context will require further testing in the future.

421 We propose that multiple weak interactions of the KIN-A C-terminal unstructured tail with
422 kinetochore components act in synergy to stabilize the CPC at kinetochores. Critically, these
423 interactions need to be of transient and reversible nature to permit the dynamic release of the CPC
424 upon anaphase onset. Three mechanisms are likely to play a role in this context (Fig. 7). First,
425 removal of the KKT8 complex (the 'CD1 receptor') at the metaphase-anaphase transition effectively
426 eliminates one of the key CPC-kinetochore interfaces. Secondly, the affinity of the KIN-A C-terminal
427 tail for its binding partners at the kinetochore may be further finetuned through reversible post-
428 translational modifications. In support of this, the KIN-A C-terminal tail harbors many pututative
429 CRK3 sites (10 sites matching the minimal S/T-P consensus motif for CDKs) and is also heavily
430 phosphorylated by Aurora B^{AUK1} in vitro (Ballmer et al., 2024). Finally, we speculate that the
431 interaction of KIN-A motor domain with microtubules, coupled to the force generating ATP
432 hydrolysis and possibly plus-end directed motion, eventually outcompetes the weakened
433 interactions of the CPC with the kinetochore and facilitates the extraction of the CPC from
434 chromosomes onto spindle microtubules during anaphase. Indeed, deletion of the KIN-A motor
435 domain or impairment of its motor function through N-terminal GFP tagging causes the CPC to be
436 trapped at kinetochores in anaphase. Central spindle localization is additionally dependent on the
437 ATPase activity of the KIN-A motor domain as illustrated by the KIN-A rigor mutant.

438 It remains to be investigated whether KIN-A functions as a plus-end directed motor. The role
439 of the KIN-B in this context is equally unclear. Because KIN-B does not possess a functional kinesin
440 motor domain, we deem it unlikely that the KIN-A:KIN-B heterodimer moves hand-over-hand along

441 microtubules as do conventional (kinesin-1 family) kinesins. Rather, the KIN-A motor domain may
442 function as a single-headed unit and drive processive plus-end directed motion using a mechanism
443 similar to the kinesin-3 family kinesin KIF1A (Okada and Hirokawa, 1999). Formation of transient
444 complexes between the CPC and kinesins or other microtubule plus-end tracking proteins upon
445 anaphase onset appears to be a common theme underlying the central spindle translocation of the
446 CPC. For instance, the CPC interacts with MKLP2 or Bim1^{EB1} in human and yeast cells, respectively
447 (Gruneberg et al., 2004; Zimniak et al., 2012). Thus, deeper understanding of the CPC regulation in
448 trypanosomes is bound to provide evolutionary insights into fundamental principles of chromosome
449 segregation in eukaryotes and can lead to the discovery of druggable targets to combat kinetoplastid
450 diseases (Saldivia et al., 2020).
451
452
453 ## Materials and Methods
454
455 **Cloning**
456 All primers, plasmids, bacmids, and synthetic DNA used in this study as well as their source or
457 construction details are described in Supplemental Table S1. All constructs were sequence verified.
458
459 **Trypanosome culture**
460 All trypanosome cell lines used in this study were derived from *T. brucei* SmOxP927 procyclic form
461 cells (TREU 927/4 expressing T7 RNA polymerase and the tetracycline repressor to allow inducible
462 expression; Poon *et al.*, 2012) or from PCF1339 procyclic form cells (TREU 927/4 expressing T7 RNA
463 polymerase, tetracycline repressor and the Cas9 nuclease, Beneke et al., 2017) and are described in
464 Supplemental Table S1. Cells were grown at 28°C in SDM-79 medium supplemented with 10%
465 (vol/vol) heat-inactivated fetal calf serum, 7.5 µg/ml hemin (Brun and Schönenberger, 1979), and
466 appropriate selection drugs. Cell growth was monitored using a CASY cell counter (Roche). PCR
467 products or plasmids linearized by NotI were transfected into cells by electroporation (Biorad).
468 Transfected cells were selected by the addition of 30 µg/ml G418 (Sigma), 25 µg/ml hygromycin
469 (Sigma), 5 µg/ml phleomycin (Sigma), or 10 µg/ml blasticidin S (Insight biotechnology). To obtain
470 endogenously tagged clonal strains, transfected cells were selected by the addition of appropriate
471 drugs and cloned by dispensing dilutions into 96-well plates. Endogenous YFP tagging was performed
472 using the pEnT5-Y vector (Kelly et al., 2007) or a PCR-based method (Dean et al., 2015). Endogenous
473 tdTomato tagging was performed using pBA148 (Akiyoshi and Gull, 2014) and its derivatives. All
474 constructs for ectopic expression of GFP fusion proteins include a short nuclear localization signal

475 (NLS) (Marchetti et al., 2000). For doxycycline inducible expression of head-to-head (pBA3-based)
476 and hairpin (pBA310-based) RNAi constructs, GFP-NLS (pBA310-based) and GFP-NLS-LacI fusion
477 proteins (pBA795-based), the linearized plasmids were integrated into 177-bp repeats on
478 minichromosomes. Expression of GFP-NLS or GFP-NLS-LacI fusions was induced by the addition of 10
479 ng/mL doxycycline for 24 h. RNAi was induced by the addition of 1 µg/ml doxycycline. LacO–LacI
480 tethering experiments were carried out as described previously using the LacO array inserted at the
481 rDNA locus (Ishii and Akiyoshi, 2020; Landeira and Navarro, 2007).
482
483 **Immunoprecipitation followed by mass spectrometry (IP-MS)**
484 For standard IPs, 400-ml cultures of asynchronously growing cells were grown to ~5 – 10 million
485 cells/ml. Cells were pelleted by centrifugation (800 g, 10 min), washed once with PBS, and extracted
486 in PEME (100 mM Pipes-NaOH, pH 6.9, 2 mM EGTA, 1 mM $MgSO_4$, and 0.1 mM EDTA) with 1% NP-
487 40, protease inhibitors (10 µg/ml leupeptin, 10 µg/ml pepstatin, 10 µg/ml E-64, and 0.2 mM PMSF)
488 and phosphatase inhibitors (1 mM sodium pyrophosphate, 2 mM Na-β-glycerophosphate, 0.1 mM
489 Na_3VO_4, 5 mM NaF, and 100 nM microcystin-LR) for 5 min at RT, followed by centrifugation at 1,800
490 g for 15 min. Samples were kept on ice from this point on. The pelleted fraction containing
491 kinetochore proteins was resuspended in modified buffer H (BH0.15: 25 mM Hepes, pH 8.0, 2 mM
492 $MgCl_2$, 0.1 mM EDTA, pH 8.0, 0.5 mM EGTA, pH 8.0, 1% NP-40, 150 mM KCl, and 15% glycerol) with
493 protease and phosphatase inhibitors. Samples were sonicated to solubilize kinetochore proteins (12
494 s, three times with 1-min intervals on ice). 12 µg of mouse monoclonal anti-GFP antibodies
495 (11814460001; Roche) preconjugated with 60 µl slurry of Protein-G magnetic beads (10004D;
496 Thermo Fisher Scientific) with dimethyl pimelimidate (Unnikrishnan et al., 2012) were incubated
497 with the extracts for 2.5 h with constant rotation, followed by four washes with modified BH0.15
498 containing protease inhibitors, phosphatase inhibitors and 2 mM DTT. Beads were further washed
499 three times with pre-elution buffer (50 mM Tris- HCl, pH 8.3, 75 mM KCl, and 1 mM EGTA). Bound
500 proteins were eluted from the beads by agitation in 60 µl of elution buffer (0.1% RapiGest
501 [186001860; Waters] and 50 mM Tris-HCl, pH 8.3) for 25 min at RT. Eluates were then incubated at
502 100°C for 5 min. Proteins were reduced with 5 mM DTT at 37°C for 30 min and alkylated with 10 mM
503 iodoacetamide at 37°C for 30 min. The reaction was quenched by adding 10 mM DTT at 37°C for 30
504 min, and 100 µl of 20 mM Tris-HCl (pH 8.3) was added. Proteins were digested overnight at 37°C
505 with 0.2 µg trypsin (Promega). Formic acid was then added to 2% and the samples were incubated at
506 37°C for 30 min to cleave RapiGest, followed by centrifugation for 10 min. The supernatant was
507 desalted over a C18 column and analyzed by electrospray tandem mass spectrometry over a 60-min
508 gradient using Q-Exactive (Thermo Fisher Scientific) at the Advanced Proteomics Facility (University

509 of Oxford). Peptides were identified by searching tandem mass spectrometry spectra against the *T.*
510 *brucei* protein database with MaxQuant (version 2.0.1) with carbamidomethyl cysteine set as a fixed
511 modification and oxidization (Met), phosphorylation (Ser, Thr, and Tyr), and acetylation (Lys) set as
512 variable modifications. Up to two missed cleavages were allowed. The first peptide tolerance was set
513 to 10 ppm. Results were filtered to remove contaminants and reverse hits. Proteins identified with
514 at least two peptides were considered as significant and shown in Table S2 (protein FDR 1%).
515
516 **Ex vivo cross-linking of the native CPC and kinetochore complexes (IP-CLMS)**
517 For cross-linking IP-MS experiments, cell cultures were scaled up to 1,600 mL. Cell cultures were
518 treated with 10 µM MG132 for 4 h to enrich for cells in metaphase. Cell lysis and
519 immunoprecipitation steps were carried out as described above. After four washes with modified
520 BH0.15 containing protease inhibitors, phosphatase inhibitors and 2 mM DTT, beads were washed
521 three times with 25 mM HEPES pH7.5, 150 mM NaCl. Proteins were then cross-linked on beads with
522 0.4 mM BS^3 (bis(sulfosuccinimidyl)suberate) (Thermo Fisher Scientific) for 30 min at RT with
523 agitation, followed by three washes in 25 mM HEPES pH7.5, 150 mM NaCl and a further three
524 washes in 0.1 M ammonium bicarbonate. Samples were then incubated in 8 M urea dissolved in 0.1
525 M ammonium bicarbonate for 10 min at RT with agitation. Proteins were reduced with 10 mM TCEP
526 for 20 min and alkylated with 10 mM iodoacetamide for 40 min at RT. Proteins were then then pre-
527 digested with 0.4 µg LysC for 2 h at 37°C. The urea concentration in the sample was brought down to
528 < 1 M by addition of 0.1 M ammonium bicarbonate before adding $CaCl_2$ (to 2 mM) and 0.7 µg of
529 trypsin for overnight digestion at 37°C. Formic acid was then added to 2% and the samples were
530 frozen. The cross-linked samples were further processed and analyzed at the proteomics core facility
531 at EMBL Heidelberg. Digested peptides were concentrated and desalted using an OASIS HLB µElution
532 Plate (Waters) according to manufacturer instructions. Crosslinked peptides were enriched using size
533 exclusion chromatography (Leitner et al., 2012). In brief, desalted peptides were reconstituted with
534 SEC buffer (30% (v/v) ACN in 0.1% (v/v) TFA) and fractionated using a Superdex Peptide PC 3.2/30
535 column (GE) on a 1200 Infinity HPLC system (Agilent) at a flow rate of 0.05 ml/min. Fractions eluting
536 between 50-70 µl were evaporated to dryness and reconstituted in 30 µl 4% (v/v) ACN in 1% (v/v)
537 FA. Collected fractions were analyzed by liquid chromatography (LC)-coupled tandem mass
538 spectrometry (MS/MS) using an UltiMate 3000 RSLC nano LC system (Dionex) fitted with a trapping
539 cartridge (µ-Precolumn C18 PepMap 100, 5µm, 300 µm i.d. x 5 mm, 100 Å) and an analytical column
540 (nanoEase M/Z HSS T3 column 75 µm x 250 mm C18, 1.8 µm, 100 Å, Waters). Trapping was carried
541 out with a constant flow of trapping solvent (0.05% trifluoroacetic acid in water) at 30 µl/min onto
542 the trapping column for 6 minutes. Subsequently, peptides were eluted and separated on the

543 analytical column using a gradient composed of Solvent A (3% DMSO, 0.1% formic acid in water) and
544 solvent B (3% DMSO, 0.1% formic acid in acetonitrile) with a constant flow of 0.3 µl/min. The outlet
545 of the analytical column was coupled directly to an Orbitrap Fusion Lumos (Thermo Scientific,
546 SanJose) mass spectrometer using the nanoFlex source. The peptides were introduced into the
547 Orbitrap Fusion Lumos via a Pico-Tip Emitter 360 µm OD x 20 µm ID; 10 µm tip (CoAnn Technologies)
548 and an applied spray voltage of 2.1 kV, instrument was operated in positive mode. The capillary
549 temperature was set at 275°C. Only charge states of 4-8 were included. The dynamic exclusion was
550 set to 30 sec. and the intensity threshold was $5e^4$. Full mass scans were acquired for a mass range
551 350-1700 m/z in profile mode in the orbitrap with resolution of 120000. The AGC target was set to
552 Standard and the injection time mode was set to Auto. The instrument was operated in data
553 dependent acquisition (DDA) mode with a cycle time of 3 sec between master scans and MSMS
554 scans were acquired in the Orbitrap with a resolution of 30000, with a fill time of up to 100 ms and a
555 limitation of $2e^5$ ions (AGC target). A normalized collision energy of 32 was applied. MS2 data was
556 acquired in profile mode. RAW MS files were searched by the pLink2 software (Chen et al., 2019),
557 with carbamidomethyl cysteine set as a fixed and oxidization (Met) set as variable modifications. Up
558 to two missed cleavages were allowed. Precursor tolerance was set to 10 ppm. All the identified
559 cross-links are shown in Table S2 (FDR 5%). Cross-links were plotted using xiView (Graham et al.,
560 2019). All raw mass spectrometry files and custom database files used in this study have been
561 deposited with the ProteomeXchange Consortium via the PRIDE partner repository (Deutsch et al.,
562 2020; Perez-Riverol et al., 2019) with the dataset identifier PXD045987.
563
564 **Fluorescence microscopy**
565 Cells were washed once with PBS, settled onto glass slides, and fixed with 4% paraformaldehyde in
566 PBS for 5 min as described previously (Nerusheva and Akiyoshi, 2016). Cells were then permeabilized
567 with 0.1% NP-40 in PBS for 5 min and embedded in mounting media (1% wt/vol 1,4-
568 diazabicyclo[2.2.2]octane, 90% glycerol, 50 mM sodium phosphate, pH 8.0) containing 100 ng/ml
569 DAPI. Images were captured on a Zeiss Axioimager.Z2 microscope (Zeiss) installed with ZEN using a
570 Hamamatsu ORCA-Flash4.0 camera with 63× objective lenses (1.40 NA). Typically, ~20 optical slices
571 spaced 0.2 or 0.24 µm apart were collected. Images were analysed in ImageJ/Fiji (Schneider et al.,
572 2012). Kinetochore localization of endogenously tagged kinetochore proteins or ectopically
573 expressed constructs were examined manually by quantifying the number of cells that clearly had
574 detectable kinetochore-like dots at indicated cell cycle stages. Shown images are central slices.
575
576 **In silico structure and interaction predictions**

577 Structures and interactions were predicted with AlphaFold2-Multimer-v2 (Evans et al., 2022; Jumper
578 et al., 2021) through ColabFold using MMseqs2 (UniRef+Environmental) and default settings
579 (Mirdita et al., 2022). Structural predictions of KIN-A/KIN-B, KIN-A$^{310-862}$/KIN-B$^{317-624}$, CPC1/CPC2/KIN-
580 A$^{300-599}$/KIN-B 317-624, and KIN-A$^{700-800}$/KKT9/KKT11 were performed using ColabFold version 1.3.0
581 (AlphaFold-Multimer version 2), while those of AUK1/CPC1/CPC2/KIN-A$^{1-599}$/KIN-B, KKT7^{1-}
582 ^{261}/KKT9/KKT11/KKT8/KKT12, KKT9/KKT11/KKT8/KKT12, and KKT7$^{1-261}$/KKT9/KKT11 were performed
583 using ColabFold version 1.5.3 (AlphaFold-Multimer version 2.3.1) using default settings, accessed via
584 https://colab.research.google.com/github/sokrypton/ColabFold/blob/v1.3.0/AlphaFold2.ipynb and
585 https://colab.research.google.com/github/sokrypton/ColabFold/blob/v1.5.3/AlphaFold2.ipynb. All
586 structure figures were made using PyMOL version 2.5.2 (Schrödinger, LLC). The following command
587 was used to map pLDDT score onto the AF2 predicted structure models: spectrum b, rainbow_rev,
588 maximum=100, minimum=50.
589
590 **Protein purification from *E. coli***
591 Recombinant 6HIS-KKT8, KKT9, KKT11, KKT12 (pBA457) and derivatives were expressed in Rosetta
592 2(DE3)pLys *E. coli* cells (Novagen). 6HIS-KIN-A$^{2-309}$ (pBA2519) and 6HIS-KIN-B$^{2-316}$ (pBA2513) were
593 expressed in BL21(DE3) cells. Proteins were purified and eluted from TALON beads as previously
594 described (Llauró et al., 2018). Briefly, cells were grown in 2xTY media at 37°C to an OD_{600} of ~0.8, at
595 which point protein expression was induced by 0.1 mM IPTG, and then incubated overnight at 20°C.
596 Cells were pelleted at 3,400 g at 4°C and pellets were resuspended in P500 buffer (50 mM sodium
597 phosphate, pH 7.5, 500 mM NaCl, 5 mM imidazole and 10% glycerol) supplemented with protease
598 inhibitors (20 µg/ml leupeptin, 20 µg/ml pepstatin, 20 µg/ml E-64, 0.4 mM PMSF) and 1 mM TCEP,
599 and were sonicated on ice. Lysates were treated with benzonase nuclease (500 U/1 l culture) and
600 spun at 48,000 g at 4°C for 30 min. Supernatant was incubated with TALON beads (Takara Clontech)
601 for 1 h at 4°C, rotating. The beads were washed three times with lysis buffer and proteins were then
602 eluted with elution buffer (P500 buffer containing 250 mM imidazole with 1 mM TCEP). For
603 microtubule co-sedimentation assays, 6HIS-KIN-A$^{2-309}$ and 6HIS-KIN-B$^{2-316}$ were buffer exchanged into
604 BRB80 (80 mM Pipes-KOH, pH 6.9, 1 mM EGTA, and 1 mM $MgCl_2$) with 100 mM KCl using a Zeba
605 columns (Thermo Fisher) and flash-frozen in liquid nitrogen for -80°C storage. Polyacrylamide gels
606 were stained with SimplyBlue SafeStain (Invitrogen).
607
608 **Microtubule co-sedimentation assay**
609 Microtubule co-sedimentation assays were performed as described previously (Ludzia et al., 2021).
610 Briefly, taxol-stabilised microtubules were prepared by mixing 2.5 ml of 100 µM porcine tubulin

611 (Cytoskeleton) resuspended in BRB80 with 1 mM GTP (Cytoskeleton), 1.25 µl BRB80, 0.5 µl of 40 mM
612 $MgCl_2$, 0.5 µl of 10 mM GTP, and 0.25 µl DMSO, and incubated for 20 min at 37C. 120 ml of pre-
613 warmed BRB80 containing 12.5 µM Taxol (paclitaxel; Sigma) was added to the sample to bring the
614 microtubule concentration to ~2 µM. 20 µl of 6HIS-KIN-A^{2-309} or 6HIS-KIN-B^{2-316} (at final
615 concentration of 4 µM) in BRB80 with 100 mM KCl were mixed with 20 µl of microtubules (final, 1
616 µM) and incubated for 45 min at room temperature. As a control, we incubated 6HIS-KIN-A^{2-309} or
617 6HIS-KIN-B^{2-316} with BRB80 (with 12.5 µM Taxol). The samples were spun at 20,000 g at room
618 temperature for 10 min, and the supernatant was collected. To the tubes containing pelleted
619 fractions, we added 40 µl of chilled BRB80 with 5 mM $CaCl_2$ and incubated on ice for 5 min to
620 depolymerise microtubules. Following the incubation, samples were boiled for 5 min before SDS-
621 PAGE. Gels were stained with SimplyBlue Safe Stain (Invitrogen). Co-sedimentation assays were
622 performed at least twice with similar results.
623
624 **Immunoblotting**
625 Cells were harvested by centrifugation (800 g, 5 min) and washed with 1 ml PBS. The pellet was
626 resuspended in 1× LDS sample buffer (Thermo Fisher) with 0.1 M DTT. Denaturation of proteins was
627 performed for 5 min at 95°C. SDS-PAGE and immunoblots were performed by standard methods
628 using the following antibodies: rabbit polyclonal anti-GFP (TP401, 1:5000) and mouse monoclonal
629 TAT1 (anti-trypanosomal-alpha-tubulin, 1:5000, a kind gift from Keith Gull) (Woods et al., 1989).
630 Secondary antibodies used were: IRDye 680RD goat anti-mouse (LI-COR, 926-68070) and IRDye
631 800CW goat anti-rabbit (LI-COR, 926-32211). Bands were visualized on an ODYSSEY Fc Imaging
632 System (LI-COR).
633
634 **Multiple sequence alignment**
635 Protein sequences and accession numbers for Aurora B^{AUK1}, $INCENP^{CPC1}$, CPC2, KIN-A and KIN-B used
636 in this study were retrieved from the TriTryp database (Aslett et al., 2010), UniProt (Bateman, 2019),
637 or a published study (Butenko et al., 2020). Searches for homologous proteins were done using
638 BLAST in the TriTryp database (Aslett et al., 2010) or using hmmsearch using manually prepared
639 hmm profiles (HMMER version 3.0; Eddy, 1998). The top hit in each organism was considered as a
640 true ortholog only if the reciprocal BLAST search returned the query protein as a top hit in *T. brucei*.
641 Multiple sequence alignment was performed with MAFFT (L-INS-i method, version 7) (Katoh et al.,
642 2019) and visualised with the Clustalx colouring scheme in Jalview (version 2.10) (Waterhouse et al.,
643 2009).
644

645

646 ## Acknowledgements

647

648 We thank Miguel Navarro (Instituto de Parasitologıá y Biomedicina López-Neyra, Consejo Superior
649 de Investigaciones Cientificas, Spain) for providing pMig75 and pMig96 plasmids and Midori Ishii
650 Kanazawa and William Carter for helping trypanosome strain construction. We thank the Micron
651 Advanced Bioimaging Unit and the Advanced Proteomics Facility at the University of Oxford, and the
652 Proteomics Core Facility at the EMBL in Heidelberg, especially Mandy Rettel and Jennifer Schwarz,
653 for their support. We also thank Patryk Ludzia and Midori Ishii Kanazawa for comments on our
654 manuscript. D. Ballmer was supported by the Berrow Foundation. B. Akiyoshi was supported by a
655 Wellcome Trust Senior Research Fellowship (grant 210622/Z/18/Z).

656

657 The authors declare no competing financial interest.

658

659 Rights retention: This research was funded in whole or in part by Wellcome Trust (grant
660 210622/Z/18/Z). For the purpose of Open Access, the author has applied a CC BY public copyright
661 licence to any Author Accepted Manuscript (AAM) version arising from this submission.

662

663 Author contributions: D. Ballmer performed essentially all experiments except for some LacI/LacO
664 tethering experiments that were performed by B. Akiyoshi. D. Ballmer wrote the manuscript. B.
665 Akiyoshi edited the manuscript.

666

667

668 ## Figure legends

669

670 **Figure 1. KIN-A and KIN-B are bona fide CPC proteins in *T. brucei*.** (A) Clustered heatmap showing
671 enrichment (log2 intensity based absolute quantification (IBAQ)) of mitotic proteins co-purifying
672 with ectopically expressed GFP-INCENP^{CPC1}, GFP-KIN-A and GFP-KIN-B. The heatmap was generated
673 using the Python Seaborn library using WPGMA clustering. Cell lines: BAP2190, BAP2286, BAP2288.
674 Immunoprecipitation was performed using anti-GFP antibodies. See Table S2 for all proteins
675 identified by mass spectrometry. (B) Cartoon depicting the kinetoplast (K) / nucleus (N) configuration
676 throughout the cell cycle in procyclic *T. brucei*, with K* denoting an elongated kinetoplast. The
677 kinetoplast is an organelle found uniquely in kinetoplastids, which contains the mitochondrial DNA
678 and replicates and segregates prior to nuclear division. The KN configuration serves as a cell cycle

679 marker (Siegel et al., 2008; Woodward and Gull, 1990). (C) to (E) Representative fluorescence
680 micrographs showing the dynamic localization of YFP-Aurora B^{AUK1} (C), KIN-A-YFP (D) and GFP-KIN-B
681 (E) over the course of the cell cycle. Kinetochores are marked with tdTomato-KKT2. DNA was stained
682 with DAPI. Cell lines: BAP1515, BAP3066, BAP2288. Scale bars, 2 µm. (F) Phylogenetic tree of
683 kinetoplastids, diplonemids and euglenids along with the presence (black dots) / absence (white
684 dots) patterns of CPC components. The phylogenetic tree of Euglenozoa is based on (Butenko et al.,
685 2020).
686
687 **Figure 2. Kinetochore localization of the CPC depends on KIN-A and KIN-B.** (A) Representative
688 fluorescence micrographs showing the localization of YFP-tagged Aurora B^{AUK1}, $INCENP^{CPC1}$, KIN-A and
689 KIN-B in 2K1N cells upon RNAi-mediated knockdown of indicated CPC subunits. Note that nuclear
690 close-ups are shown here. CPC proteins were not detected in the cytoplasm. RNAi was induced with
691 1 µg/mL doxycycline for 24 h (KIN-B RNAi) or 16 h (all others). Cell lines: BAP3092, BAP2552,
692 BAP2557, BAP3093, BAP2906, BAP2900, BAP2904, BAP3094, BAP2899, BAP2893, BAP2897,
693 BAP3095, BAP3096, BAP2560, BAP2564, BAP3097. Scale bars, 2 µm. (B) to (E) Quantification of 2K1N
694 cells that have kinetochore-like dots of YFP-tagged Aurora B^{AUK1} (B), $INCENP^{CPC1}$ (C), KIN-A (D) and
695 KIN-B (E) upon RNAi-mediated depletion of indicated CPC components. All graphs depict the means
696 (bar) ± SD of at least two replicates (shown as dots). A minimum of 100 cells per replicate were
697 quantified. * $P < 0.05$, ** $P \leq 0.01$, *** $P \leq 0.001$ (two-sided, unpaired t-test). (F) to (H)
698 Representative fluorescence micrographs showing the localization of ectopically expressed GFP-KIN-
699 A^{fl} (F), -KIN-A^{2-309} (G) and -KIN-$A^{310-862}$ (H). Expression of GFP fusion proteins was induced with 10
700 ng/mL doxycycline for 24 h. Kinetochores are marked with tdTomato-KKT2. Arrowheads indicate
701 KIN-A^{fl} and KIN-$A^{310-862}$ signals at kinetochores. KIN-A^{2-309} is found at mitotic spindle during
702 metaphase. Cell lines: BAP2286, BAP2297, BAP2287. Scale bars, 2 µm
703
704 **Figure 3. Structural model of the trypanosome CPC.** (A) Circular view of the BS^3 crosslinks observed
705 between the subunits of the trypanosome CPC, obtained from native complexes isolated by
706 immunoprecipitation of YFP-Aurora B^{AUK1} (Cell line: BAP2198). pLink2 (Chen et al., 2019) was used to
707 obtain crosslinks from mass spectrometry data. xiView (Graham et al., 2019) was used for data
708 visualization. Only crosslinks with a score better than E^{-3} are shown. See Table S2 for all crosslinks
709 identified by mass spectrometry. (B) Cartoon representation showing two orientations of the
710 trypanosome CPC, coloured by protein on the left (Aurora B^{AUK1}: crimson, $INCENP^{CPC1}$: green, CPC2:
711 cyan, KIN-A: magenta, and KIN-B: yellow) or according to their pLDDT values on the right, assembled
712 from AlphaFold2 predictions shown in Figure S3. The pLDDT score is a per-residue estimate of the

713 confidence in the AlphaFold prediction on a scale from 0 – 100. pLDDT > 70 (blue, cyan) indicates a
714 reasonable accuracy of the model, while pLDDT < 50 (red) indicates a low accuracy and often reflects
715 disordered regions of the protein (Jumper et al., 2021). BS^3 crosslinks in (B) were mapped onto the
716 model using PyXlinkViewer (blue = distance constraints satisfied, red = distance constraints violated,
717 Cα-Cα Euclidean distance threshold = 30 Å) (Schiffrin et al., 2020).
718
719 **Figure 4. The CPC is recruited to kinetochores via the KKT7 – KKT8 complex pathway.** (A)
720 Representative fluorescence micrographs showing the localization of YFP-Aurora B^{AUK1} upon RNAi-
721 mediated knockdown of KKT7. RNAi was induced with 1 µg/mL doxycycline for 24 h. Cell line:
722 BAP577. Scale bars, 2 µm. (B) Quantification of 2K1N cells that have kinetochore-like dots of YFP-
723 Aurora B^{AUK1} upon knockdown of KKT7. All graphs depict the means (bar) ± SD of three replicates
724 (shown as dots). A minimum of 50 cells per replicate were quantified. *** $P \leq 0.001$ (two-sided,
725 unpaired t-test). (C) Representative fluorescence micrographs showing the localization of YFP-Aurora
726 B^{AUK1} upon RNAi-mediated knockdown of KKT9. RNAi was induced with 1 µg/mL doxycycline for 24 h.
727 Kinetochores are marked with tdTomato-KKT2. Cell line: BAP2276. Scale bars, 2 µm. (D)
728 Quantification of 2K1N cells that have kinetochore-like dots of YFP-Aurora B^{AUK1} upon knockdown of
729 KKT9. All graphs depict the means (bar) ± SD of three replicates (shown as dots). A minimum of 50
730 cells per replicate were quantified. *** $P \leq 0.001$ (two-sided, unpaired t-test). (E) and (F)
731 Representative micrographs of cells in S phase and anaphase showing recruitment of tdTomato-
732 Aurora B^{AUK1} to LacO foci marked by ectopically expressed GFP-$KKT7^{2-261}$-LacI (E) or -KKT8-LacI (F).
733 The insets show the magnification of the boxed region. Expression of LacI fusion proteins was
734 induced with 10 ng/mL doxycycline for 24 h. Arrowheads in (F) indicate anaphase kinetochore
735 localization of GFP-KKT8-LacI and tdTomato-Aurora B^{AUK1}. Anaphase kinetochore localization of
736 tdTomato-Aurora B^{AUK1} was observed in 75% of anaphase cells expressing GFP-KKT8-LacI (n = 28).
737 Cell lines: BAP1395, BAP2640. Scale bars, 2 µm. Of note, LacI fusions with $INCENP^{CPC1}$, KIN-A and KIN-
738 B constructs robustly localized to kinetochores like their endogenous counterparts and failed to form
739 distinct LacI foci and could therefore not be used to assess ectopic recruitment of KKT proteins. (G)
740 AlphaFold2 model of the KKT7 – KKT8 complex, coloured by protein ($KKT7^{1-261}$: green, KKT8: blue,
741 KKT12: pink, KKT9: cyan and KKT11: orange) (left) and by pLDDT (center). BS^3 crosslinks in (H) were
742 mapped onto the model using PyXlinkViewer (Schiffrin et al., 2020) (blue = distance constraints
743 satisfied, red = distance constraints violated, Cα-Cα Euclidean distance threshold = 30 Å). Right:
744 Predicted Aligned Error (PAE) plot of model shown on the left (rank_2). The colour indicates
745 AlphaFold's expected position error (blue = low, red = high) at the residue on the x axis if the
746 predicted and true structures were aligned on the residue on the y axis (Jumper et al., 2021). (H)

747 Circular view of the BS^3 crosslinks observed among KKT7 and KKT8 complex subunits, obtained from
748 native complexes isolated by immunoprecipitation of YFP-tagged KKIP1 (Cell line: BAP710a). pLink2
749 (Chen et al., 2019) was used to obtain crosslinks from mass spectrometry data and xiView (Graham
750 et al., 2019) was used for data visualization. Only crosslinks with a score better than E^{-3} are shown.
751 See Table S2 for all crosslinks identified by mass spectrometry. (I) Indicated combinations of 6HIS-
752 tagged KKT8 (~46 kDa), KKT9 (~39 kDa), KKT11 (~29 kDa) and KKT12 (~23 kDa) were co-expressed in
753 *E. coli*, followed by metal affinity chromatography and SDS-PAGE. The asterisk indicates a common
754 contaminant.
755
756 **Figure 5. Two conserved domains within the C-terminal tail of KIN-A promote kinetochore**
757 **recruitment of the CPC.** (A) Left: AlphaFold2 model of KKT9:KKT11 in complex with KIN-$A^{700-862}$.
758 Cartoon representations are coloured by protein (KKT9: cyan, KKT11: orange, KIN-A: magenta) (left)
759 or according to their pLDDT values (blue = high confidence, red = low confidence) (center). Right:
760 Predicted Aligned Error (PAE) plot of model (rank_1) predicted by AlphaFold2 (blue = high
761 confidence, red = low confidence in the relative positions of the domains to one another). CD1 of
762 KIN-A was predicted to interact with KKT9:KKT11 in all five AlphaFold2 models (rank_1 to rank_5).
763 (B) Multiple sequence alignment of KIN-A CD1 and CD2 showing conservation. (C) to (E)
764 Representative fluorescence micrographs showing the localization of tdTomato-Aurora B^{AUK1} and
765 YFP-tagged KIN-A^{wt} (C), KIN-$A^{\Delta CD1\ (717–743)}$ (D) and KIN-$A^{\Delta CD2\ (816–862)}$ (E). RNAi was induced with 1 µg/mL
766 doxycycline for 24 h to deplete the untagged KIN-A allele. Cell lines: BAP3067, BAP3128, BAP3127.
767 Scale bars, 2 µm. (F) Stacked bar charts showing the percentage of YFP-tagged KIN-A^{wt}, KIN-$A^{\Delta CD1}$ and
768 KIN-$A^{\Delta CD2}$ on kinetochores, kinetochores + spindle and spindle only in metaphase cells. Examples and
769 schematic illustrations of the three categories used for scoring are presented on the left. A minimum
770 of 50 cells per condition were quantified. (G) Stacked bar charts showing the percentage of
771 tdTomato-Aurora B^{AUK1} on kinetochores, kinetochores + spindle and spindle only in metaphase cells
772 upon rescue with YFP-tagged KIN-A^{wt}, KIN-$A^{\Delta CD1}$ or KIN-$A^{\Delta CD2}$. A minimum of 50 cells per condition
773 were quantified. (H) Growth curves for indicated cell lines and conditions. RNAi was induced with 1
774 µg/mL doxycycline for to deplete the untagged KIN-A allele in the knockdown conditions and
775 cultures were diluted at day 2. Cell lines: BAP3067, BAP3128, BAP3127.
776
777 **Figure 6. KIN-A ATPase activity is required for central spindle localization of the CPC in anaphase.**
778 (A) Multiple sequence alignment showing conservation of Switch II region in KIN-A and KIN-B, with
779 the key glycine residue (G210 in *T. brucei*) targeted for rigor mutation highlighted in red. (B)
780 Representative fluorescence micrographs showing the localization of tdTomato-MAP103 (spindle

781 marker) and YFP-tagged KIN-A^{wt} or KIN-A^{G210A} (rigor mutant). RNAi was induced with 1 µg/mL
782 doxycycline for 24 h to deplete the untagged KIN-A allele. Cell lines: BAP3068, BAP3071. Scale bars, 2
783 µm. (C) Quantification showing the percentage of anaphase cells that have YFP-tagged KIN-A^{wt} or
784 KIN-A^{G210A} localized at the central spindle. All graphs depict the means (bar) ± SD of three replicates
785 (shown as dots). A minimum of 40 cells per replicate were quantified. *** $P \leq 0.001$ (two-sided,
786 unpaired t-test). (D) and (E) Representative fluorescence micrographs showing the localization of
787 tdTomato-Aurora B^{AUK1} and YFP-tagged KIN-A^{wt} (D) or KIN-A^{G210A} (E). RNAi was induced with 1 µg/mL
788 doxycycline for 24 h to deplete the untagged KIN-A allele. Cell lines: BAP3067, BAP3070. Scale bars, 2
789 µm. (F) Quantification showing the percentage of anaphase cells that have tdTomato-Aurora B^{AUK1}
790 localized at the central spindle upon rescue with YFP-tagged KIN-A^{wt} or KIN-A^{G210A}. Graphs for the
791 KIN-A^{G210} rescue conditions (grey) depict the means (bar) ± SD of three replicates (shown as dots). A
792 minimum of 30 cells per replicate were quantified. (G) Growth curves for indicated cell lines and
793 conditions. RNAi was induced with 1 µg/mL doxycycline for to deplete the untagged KIN-A allele in
794 the knockdown conditions and cultures were diluted at day 2. Cell lines: BAP3064, BAP3065. (H) Cell
795 cycle profiles for the indicated cell lines and conditions. RNAi was induced with 1 µg/mL doxycycline
796 to deplete the untagged KIN-A allele in the knockdown conditions and cells were fixed after 24 h. All
797 graphs depict the means (bar) ± SD of at least two replicates. A minimum of 300 cells per replicate
798 were quantified. Cell lines: BAP3064, BAP3065. *** $P \leq 0.001$ (two-sided, unpaired t-test).
799
800 **Figure 7. Model for CPC localization and function in trypanosomes.** (A) KIN-A (magenta) and KIN-B
801 (yellow) interact via their coiled-coil domains and form a scaffold for the assembly of CPC2 (cyan)
802 and the catalytic module of the CPC, composed of Aurora B^{AUK1} (red) and INCENP^{CPC1} (green). During
803 interphase, the catalytic module is positioned close to the kinesin head domains of KIN-A and KIN-B.
804 CPC recruitment to the inner kinetochore is mediated through multiple weak interactions between
805 the C-terminal unstructured tail of KIN-A, containing CD1 and CD2, with the coiled-coil domain of
806 KKT9:KKT11 (dark blue:light blue) and possibly the N-terminus of KKT7 (blue). The KKT8 complex,
807 comprising KKT9:KKT11 and KKT8:KKT12 (dark grey:light grey) subcomplexes, is connected to other
808 kinetochore proteins through KKT7. Additional kinetochore targeting domains of the CPC may reside
809 within the C-terminus of KIN-B and/or CPC2. We propose that the KIN-A:KIN-B subcomplex
810 represents the main localization module of the trypanosome CPC. As illustrated in (B), the affinity of
811 the KIN-A C-terminal tail for its receptor(s) at the kinetochore may be further modulated through
812 phosphorylation by the CDK1 homolog CRK3 and the Aurora B^{AUK1} kinase itself (Ballmer et al., 2024).
813 Interaction of the N-terminal motor domain of KIN-A with spindle microtubules (MTs) from
814 prometaphase onwards causes the catalytic module to disengage from its kinesin head-associated

815 state. The ~100 amino acid long flexible linker within INCENP^{CPC1} would then permit Aurora B^{AUK1} to
816 phosphorylate its substrates within a larger but nevertheless spatially constrained target area while
817 still being anchored to the kinetochore via KIN-A:KIN-B. The motor domain of KIN-A could thus act as
818 built-in sensor for KT-MT attachments. (C) We propose that the trypanosome CPC is recruited to
819 kinetochores via the KKT7-KKT8 complex pathway (dashed arrow) and that motor activity of KIN-A
820 promotes congression of kinetochores to the metaphase plate during early mitosis. The KKT8
821 complex dissociates from kinetochores at the metaphase-to-anaphase transition and is possibly
822 degraded in an APC/C-dependend manner. Elimination of the KKT8 complex, the primary
823 kinetochore receptor of the CPC, coupled to MT binding and motor activity of the KIN-A motor
824 domain strips the CPC off kinetochores and facilitates its translocation to the central spindle in
825 anaphase.
826
827 **Figure S1. KIN-A and KIN-B are bona fide CPC proteins in *T. brucei*.** (A) Heatmap showing
828 enrichment (log2 intensity based absolute quantification (IBAQ)) of the top 30 proteins, excluding
829 ribosomal proteins, co-purifying with YFP-Aurora B^{AUK1}. Cell line: BAP73. Immunoprecipitation was
830 performed using anti-GFP antibodies. See Table S2 for all proteins identified by mass spectrometry.
831 (B) and (C) Representative fluorescence micrographs showing the localization of tdTomato-Aurora
832 B^{AUK1} and KIN-A-YFP (B) and YFP-KIN-B (C) in late anaphase and telophase cells. Arrows indicate the
833 population of CPC proteins localized to the new FAZ tip. DNA was stained with DAPI. Cell lines:
834 BAP3067, BAP2528. Scale bars, 2 µm.
835
836 **Figure S2. Depletion of CPC proteins causes growth defects and cell cycle arrest.** (A) Growth curves
837 upon RNAi-mediated knockdown of indicated CPC subunits. Data are presented as the mean ± SD of
838 at least three replicates. RNAi was induced with 1 µg/mL doxycycline and cultures were diluted at
839 day 2. CDS stands for coding sequence, UTR for untranslated region. Cell lines: BAP941, BAP2250,
840 BAP2251, BAP2557, BAP2558, BAP3076. (B) Cell cycle profiles upon knockdown of indicated CPC
841 subunits. RNAi was induced with 1 µg/mL doxycycline and cells were fixed at 16h (for Aurora B^{AUK1},
842 INCENP^{CPC1} and KIN-A RNAi) or 24 h (CPC2 and KIN-B RNAi). All graphs depict the means (bar) ± SD of
843 at least two replicates. A minimum of 150 cells per replicate were quantified. Cell lines: BAP3092,
844 BAP2554, BAP2557, BAP3093. (C) Western Blot showing levels of YFP-tagged KIN-A or KIN-B upon
845 RNAi-mediated knockdown of KIN-B and KIN-A, respectively. RNAi was induced with 1 µg/mL
846 doxycycline for 16 h (KIN-A) or 24 h (KIN-B). Proteins were detected using anti GFP-antibodies.
847 Asterisk indicates unspecific band. Cell lines: BAP3095, BAP2564. (D) to (F) Representative
848 fluorescence micrographs showing the localization of ectopically expressed GFP-KIN-B^{fl} (D), -KIN-B^{2-}

849 ^{316} (E) and -KIN-B$^{317-624}$ (F). Expression of GFP fusion proteins was induced with 10 ng/mL doxycycline
850 for 24 h. Kinetochores are marked with tdTomato-KKT2. Cell lines: BAP2288, BAP2289, BAP2290.
851 Scale bars, 2 µm.
852
853 **Figure S3. AlphaFold2 models of CPC subcomplexes and localization of CPC1 and CPC2 truncations.**
854 (A) to (D) Cartoon representations coloured by protein (left) and pLDDT (center), and PAE plots
855 (right) of AlphaFold2 predictions for indicated CPC subcomplexes. (E) to (J) Representative
856 fluorescence micrographs showing the localization of ectopically expressed GFP-INCENP$^{CPC1\ fl}$ (E), -
857 INCENP$^{CPC1\ 2-147}$ (F), -INCENP$^{CPC1\ 2-147}$ (G), -CPC2^{fl} (H), -CPC2$^{2-120}$ (I) and -CPC2$^{121-250}$ (J) in different cell
858 cycle stages. Expression of GFP fusion proteins was induced with 10 ng/mL doxycycline for 24 h.
859 Kinetochores are marked with tdTomato-KKT2. Cell lines: BAP2190, BAP2191, BAP2193, BAP2194,
860 BAP2195, BAP2196. Scale bars, 2 µm.
861
862 **Figure S4. Kinetochore localization of Aurora B^{AUK1} and KIN-A depends on the KKT7 – KKT8 complex**
863 **pathway.** (A) Representative fluorescence micrographs showing the localization of YFP-Aurora B^{AUK1}
864 upon RNA-mediated knockdown of indicated KKT proteins. RNAi was induced with 1 µg/mL
865 doxycycline for 24 h. Cell lines: BAP3132, BAP576, BAP2551, BAP2550, BAP3133, BAP1019, BAP2549,
866 BAP2446. Scale bars, 2 µm. (B) Quantification of 2K1N cells that have kinetochore-like dots of YFP-
867 Aurora B^{AUK1} upon knockdown of indicated KKT proteins. A minimum of 40 cells per replicate were
868 examined. (C) Representative fluorescence micrographs showing the localization of KIN-A-YFP upon
869 RNA-mediated knockdown of KKT8 complex subunits. RNAi was induced with 1 µg/mL doxycycline
870 for 24 h. Cell lines: BAP2970, BAP2968, BAP2969, BAP2971. Scale bars, 2 µm. (D) Quantification of
871 2K1N cells that have kinetochore-like dots of KIN-A-YFP upon knockdown of indicated KKT8 complex
872 subunits. All graphs depict the means (bar) ± SD of at least two replicates (shown as dots). A
873 minimum of 50 cells per replicate were quantified. (E) Representative micrographs showing
874 recruitment of tdTomato-tagged KKT8, KKT9 and KKT12 to LacO foci marked by ectopically expressed
875 GFP-KKT7$^{2-261}$-LacI. Expression of GFP fusion proteins was induced with 10 ng/mL doxycycline for 24
876 h. Cell lines: BAP871, BAP873, BAP874. Scale bars, 2 µm. (F) Representative fluorescence micrograph
877 of an anaphase cell showing localization of tdTomato-KKT8 and ectopically expressed GFP-KIN-A. The
878 insets show the magnification of the boxed region. Expression of GFP-KIN-A was induced with 10
879 ng/mL doxycycline for 24 h. Cell line: BAP3080. Scale bars, 2 µm. (G) and (H) Cartoon representations
880 coloured by protein (left) and pLDDT (center), and PAE plots (right) of AlphaFold2 predictions for
881 indicated protein complexes. (I) Representative fluorescence micrographs showing localization of
882 YFP-tagged KKT8, KKT12 and KKT9 upon RNAi-mediated knockdown of indicated KKT8 complex

883 subunits. RNAi was induced with 1 µg/mL doxycycline for 24 h. Cell lines: BAP2954, BAP2952,
884 BAP2953, BAP2955, BAP2966, BAP2964, BAP2965, BAP2967, BAP2958, BAP2956, BAP2957,
885 BAP2959. Scale bars, 2 µm. (J) to (L) Quantification of 1K*1N and 2K1N cells that have kinetochore-
886 like dots of YFP-tagged KKT8 (J), KKT12 (K) and KKT9 (L) upon knockdown of indicated KKT8 complex
887 subunits. All graphs depict the means (bar) ± SD of at least three technical replicates (shown as dots)
888 from one experiment. A minimum of 100 cells per replicate were quantified. ** $P \leq 0.01$,
889 *** $P \leq 0.001$ (two-sided, unpaired t-test).
890
891 **Figure S5. CD1 and CD2 contribute synergistically to kinetochore localization of KIN-A.** (A) Multiple
892 sequence alignment of KIN-A. (B) PAE (left) and pLDDT plots (right) of AlphaFold2 predictions rank1
893 to rank5 for KIN-A$^{700-800}$ in complex with KKT9 and KKT11. (C) to (F) Representative fluorescence
894 micrographs showing the localization of ectopically expressed GFP-KIN-A$^{310-862}$ (C), -KIN-A$^{310-862\ \Delta CD2}$
895 (D) and -KIN-B$^{310-862\ \Delta CD1}$ (E) and -KIN-A$^{310-716}$ (F). Expression of GFP fusion proteins was induced with
896 10 ng/mL doxycycline for 24 h. Kinetochores are marked with tdTomato-KKT2. Cell lines: BAP2287,
897 BAP2948, BAP2949, BAP2947. Scale bars, 2 µm. (G) Quantification of metaphase (left) and anaphase
898 (right) cells that have kinetochore-like dots of indicated GFP fusion proteins. All graphs depict the
899 means (bar) ± SD of three replicates (shown as dots). A minimum of 150 cells per replicate were
900 quantified. *** $P \leq 0.001$ (two-sided, unpaired t-test). (H) Stacked bar charts showing the percentage
901 of KIN-A$^{\Delta CD1}$-YFP (left) or tdTomato-Aurora B^{AUK1} (right) on kinetochores, kinetochores + spindle and
902 spindle in KIN-A$^{\Delta CD1}$ metaphase cells with and without KIN-A RNAi. A minimum of 70 cells per
903 condition were quantified. Cell line: BAP3128. (I) Cell cycle profiles for the indicated cell lines and
904 conditions. RNAi was induced with 1 µg/mL doxycycline to deplete the untagged KIN-A allele in the
905 knockdown conditions and cells were fixed after 24 h. All graphs depict the means (bar) ± SD of three
906 replicates. A minimum of 500 cells per replicate were quantified. Cell lines: BAP3067, BAP3127,
907 BAP3128.
908
909 **Figure S6. ATPase activity of KIN-A promotes kinetochore alignment at the metaphase plate.** (A)
910 Multiple sequence alignment of KIN-A and KIN-B from different kinetoplastids, human Kinesin-1,
911 human Mklp2, and yeast Klp9. (B) Microtubule co-sedimentation assay with 6HIS-KIN-A$^{2-309}$ (left) and
912 6HIS-KIN-B$^{2-316}$ (right). S and P correspond to supernatant and pellet fractions, respectively. Note
913 that both constructs to some extent sedimented even in the absence of microtubules. Hence, lack of
914 microtubule binding for KIN-B may be due to the unstable non-functional protein used in this study.
915 (C) and (D) Representative fluorescence micrographs showing localization of YFP-tagged KIN-A (C)
916 and KIN-A^{G210A} (rigor mutant) (D) in G2 and metaphase. Kinetochores are marked with tdTomato-

917 KKT2. Cell lines: BAP3066, BAP3069. Scale bars, 2 µm. (E) and (F) Upper: Representative fluorescence
918 micrographs showing localization of YFP-tagged KIN-A (E) and KIN-A^{G210A} (rigor mutant) (F) in
919 metaphase. The mitotic spindle is marked with tdTomato-MAP103. Bounding boxes indicate area
920 used for generation of intensity profiles in FIJI/Image J. Cell lines: BAP3068, BAP3071. Scale bars, 2
921 µm. Lower: Example of 1D intensity profiles and corresponding heatmaps from the example cells
922 shown above. (G) and (H) Kinetochore alignment profiles for YFP-tagged KIN-A (G) and KIN-A^{G210A} (H).
923 RNAi was induced with 1 µg/mL doxycycline for 24 h to deplete the untagged KIN-A allele and cells
924 were treated with 10 µM MG132 for 4 h prior to fixing to prevent anaphase entry (Hayashi and
925 Akiyoshi, 2018). WPGMA clustering was performed using the Python Seaborn library. Cell lines:
926 BAP3064, BAP3065.
927
928
929 **References**
930

931 Abad MA, Gupta T, Hadders MA, Meppelink A, Wopken JP, Blackburn E, Zou J, Gireesh A, Buzuk L,
932 Kelly DA, McHugh T, Rappsilber J, Lens SMA, Jeyaprakash AA. 2022. Mechanistic basis for Sgo1-
933 mediated centromere localization and function of the CPC. *Journal of Cell Biology* **221**.
934 doi:10.1083/JCB.202108156/213318
935 Adams RR, Maiato H, Earnshaw WC, Carmena M. 2001. Essential Roles of Drosophila Inner
936 Centromere Protein (Incenp) and Aurora B in Histone H3 Phosphorylation, Metaphase
937 Chromosome Alignment, Kinetochore Disjunction, and Chromosome Segregation. *Journal of*
938 *Cell Biology* **153**:865–880. doi:10.1083/JCB.153.4.865
939 Adams RR, Wheatleya SP, Gouldsworthy AM, Kandels-Lewis SE, Carmena M, Smythe C, Gerloff DL,
940 Earnshaw WC. 2000. INCENP binds the Aurora-related kinase AIRK2 and is required to target it
941 to chromosomes, the central spindle and cleavage furrow. *Current Biology* **10**.
942 doi:10.1016/S0960-9822(00)00673-4
943 Akiyoshi B. 2020. Analysis of a Mad2 homolog in *Trypanosoma brucei* provides possible hints on the
944 origin of the spindle checkpoint. *bioRxiv*.
945 Akiyoshi B, Gull K. 2014. Discovery of Unconventional Kinetochores in Kinetoplastids. *Cell* **156**.
946 doi:10.1016/j.cell.2014.01.049
947 Allshire RC, Karpen GH. 2008. Epigenetic regulation of centromeric chromatin: old dogs, new tricks?
948 *Nat Rev Genet* **9**. doi:10.1038/nrg2466
949 Aslett M, Aurrecoechea C, Berriman M, Brestelli J, Brunk BP, Carrington M, Depledge DP, Fischer S,
950 Gajria B, Gao X, Gardner MJ, Gingle A, Grant G, Harb OS, Heiges M, Hertz-Fowler C, Houston R,
951 Innamorato F, Iodice J, Kissinger JC, Kraemer E, Li W, Logan FJ, Miller JA, Mitra S, Myler PJ,
952 Nayak V, Pennington C, Phan I, Pinney DF, Ramasamy G, Rogers MB, Roos DS, Ross C, Sivam D,
953 Smith DF, Srinivasamoorthy G, Stoeckert CJ, Subramanian S, Thibodeau R, Tivey A, Treatman C,
954 Velarde G, Wang H. 2010. TriTrypDB: a functional genomic resource for the Trypanosomatidae.
955 *Nucleic Acids Res* **38**. doi:10.1093/NAR/GKP851
956 Ballmer D, Lou HJ, Ishii M, Turk BE, Akiyoshi B. 2024. An unconventional regulatory circuitry involving
957 Aurora B controls anaphase onset and error-free chromosome segregation in trypanosomes.
958 *bioRxiv* 2024.01.20.576407. doi:10.1101/2024.01.20.576407
959 Bateman A. 2019. UniProt: a worldwide hub of protein knowledge. *Nucleic Acids Res* **47**:D506–D515.
960 doi:10.1093/NAR/GKY1049

961 Beneke T, Madden R, Makin L, Valli J, Sunter J, Gluenz E. 2017. A CRISPR Cas9 high-throughput
962 genome editing toolkit for kinetoplastids. *R Soc Open Sci* **4**:1–16. doi:10.1098/RSOS.170095
963 Berriman M, Ghedin E, Hertz-Fowler C, Blandin G, Renauld H, Bartholomeu DC, Lennard NJ, Caler E,
964 Hamlin NE, Haas B, Böhme U, Hannick L, Aslett MA, Shallom J, Marcello L, Hou L, Wickstead B,
965 Alsmark UCM, Arrowsmith C, Atkin RJ, Barron AJ, Bringaud F, Brooks K, Carrington M,
966 Cherevach I, Chillingworth TJ, Churcher C, Clark LN, Corton CH, Cronin A, Davies RM, Doggett J,
967 Djikeng A, Feldblyum T, Field MC, Fraser A, Goodhead I, Hance Z, Harper D, Harris BR, Hauser H,
968 Hostetler J, Ivens A, Jagels K, Johnson D, Johnson J, Jones K, Kerhornou AX, Koo H, Larke N,
969 Landfear S, Larkin C, Leech V, Line A, Lord A, MacLeod A, Mooney PJ, Moule S, Martin DMA,
970 Morgan GW, Mungall K, Norbertczak H, Ormond D, Pai G, Peacock CS, Peterson J, Quail MA,
971 Rabbinowitsch E, Rajandream MA, Reitter C, Salzberg SL, Sanders M, Schobel S, Sharp S,
972 Simmonds M, Simpson AJ, Tallon L, Turner CMR, Tait A, Tivey AR, Van Aken S, Walker D,
973 Wanless D, Wang S, White B, White O, Whitehead S, Woodward J, Wortman J, Adams MD,
974 Embley TM, Gull K, Ullu E, Barry JD, Fairlamb AH, Opperdoes F, Barrell BG, Donelson JE, Hall N,
975 Fraser CM, Melville SE, El-Sayed NM. 2005. The genome of the African trypanosome
976 *Trypanosoma brucei*. *Science* **309**:416–422. doi:10.1126/SCIENCE.1112642
977 Bishop JD, Schumacher JM. 2002. Phosphorylation of the Carboxyl Terminus of Inner Centromere
978 Protein (INCENP) by the Aurora B Kinase Stimulates Aurora B Kinase Activity. *Journal of*
979 *Biological Chemistry* **277**. doi:10.1074/jbc.C200307200
980 Black BE, Cleveland DW. 2011. Epigenetic Centromere Propagation and the Nature of CENP-A
981 Nucleosomes. *Cell* **144**. doi:10.1016/j.cell.2011.02.002
982 Broad AJ, DeLuca KF, DeLuca JG. 2020. Aurora B kinase is recruited to multiple discrete kinetochore
983 and centromere regions in human cells. *J Cell Biol* **219**. doi:10.1083/JCB.201905144
984 Brun R, Schönenberger M. 1979. Cultivation and in vitro cloning or procyclic culture forms of
985 *Trypanosoma brucei* in a semi-defined medium. *Acta Trop* **36**:289–292.
986 Butenko A, Opperdoes FR, Flegontova O, Horák A, Hampl V, Keeling P, Gawryluk RMR, Tikhonenkov
987 D, Flegontov P, Lukeš J. 2020. Evolution of metabolic capabilities and molecular features of
988 diplonemids, kinetoplastids, and euglenids. *BMC Biology 2020 18:1* **18**:1–28.
989 doi:10.1186/S12915-020-0754-1
990 Campbell CS, Desai A. 2013. Tension sensing by Aurora B kinase is independent of survivin-based
991 centromere localization. *Nature 2013 497:7447* **497**:118–121. doi:10.1038/nature12057
992 Carmena M, Wheelock M, Funabiki H, Earnshaw WC. 2012. The chromosomal passenger complex
993 (CPC): from easy rider to the godfather of mitosis. *Nat Rev Mol Cell Biol* **13**.
994 doi:10.1038/nrm3474
995 Cavalier-Smith T. 2010. Kingdoms Protozoa and Chromista and the eozoan root of the eukaryotic
996 tree. *Biol Lett* **6**:342–345. doi:10.1098/RSBL.2009.0948
997 Cheeseman IM, Chappie JS, Wilson-Kubalek EM, Desai A. 2006. The Conserved KMN Network
998 Constitutes the Core Microtubule-Binding Site of the Kinetochore. *Cell* **127**.
999 doi:10.1016/j.cell.2006.09.039
1000 Chen ZL, Meng JM, Cao Y, Yin JL, Fang RQ, Fan SB, Liu C, Zeng WF, Ding YH, Tan D, Wu L, Zhou WJ, Chi
1001 H, Sun RX, Dong MQ, He SM. 2019. A high-speed search engine pLink 2 with systematic
1002 evaluation for proteome-scale identification of cross-linked peptides. *Nature Communications*
1003 *2019 10:1* **10**:1–12. doi:10.1038/s41467-019-11337-z
1004 Cho US, Harrison SC. 2011. Ndc10 is a platform for inner kinetochore assembly in budding yeast. *Nat*
1005 *Struct Mol Biol* **19**:48–56. doi:10.1038/NSMB.2178
1006 Cooke CA, Heck MMS, Earnshaw WC. 1987. The inner centromere protein (INCENP) antigens:
1007 movement from inner centromere to midbody during mitosis. *J Cell Biol* **105**:2053–2067.
1008 doi:10.1083/JCB.105.5.2053
1009 Cormier A, Drubin DG, Barnes G. 2013. Phosphorylation regulates kinase and microtubule binding
1010 activities of the budding yeast chromosomal passenger complex in vitro. *J Biol Chem*
1011 **288**:23203–23211. doi:10.1074/JBC.M113.491480

1012 D'Archivio S, Wickstead B. 2017. Trypanosome outer kinetochore proteins suggest conservation of
1013 chromosome segregation machinery across eukaryotes. *Journal of Cell Biology* **216**.
1014 doi:10.1083/jcb.201608043
1015 Dean S, Sunter J, Wheeler RJ, Hodkinson I, Gluenz E, Gull K. 2015. A toolkit enabling efficient,
1016 scalable and reproducible gene tagging in trypanosomatids. *Open Biol* **5**.
1017 doi:10.1098/RSOB.140197
1018 Deutsch EW, Bandeira N, Sharma V, Perez-Riverol Y, Carver JJ, Kundu DJ, García-Seisdedos D,
1019 Jarnuczak AF, Hewapathirana S, Pullman BS, Wertz J, Sun Z, Kawano S, Okuda S, Watanabe Y,
1020 Hermjakob H, Maclean B, Maccoss MJ, Zhu Y, Ishihama Y, Vizcaíno JA. 2020. The
1021 ProteomeXchange consortium in 2020: enabling 'big data' approaches in proteomics. *Nucleic*
1022 *Acids Res* **48**:D1145. doi:10.1093/NAR/GKZ984
1023 Drinnenberg IA, Akiyoshi B. 2017. Evolutionary Lessons from Species with Unique Kinetochores. *Prog*
1024 *Mol Subcell Biol* **56**:111–138. doi:10.1007/978-3-319-58592-5_5/TABLES/1
1025 Eddy SR. 1998. Profile hidden Markov models. *Bioinformatics* **14**:755–763.
1026 doi:10.1093/BIOINFORMATICS/14.9.755
1027 Endow SA, Kull FJ, Liu H. 2010. Kinesins at a glance. *J Cell Sci* **123**:3420. doi:10.1242/JCS.064113
1028 Evans R, O'neill M, Pritzel A, Antropova N, Senior A, Green T, Žídek A, Bates R, Blackwell S, Yim J,
1029 Ronneberger O, Bodenstein S, Zielinski M, Bridgland A, Potapenko A, Cowie A,
1030 Tunyasuvunakool K, Jain R, Clancy E, Kohli P, Jumper J, Hassabis D. 2022. Protein complex
1031 prediction with AlphaFold-Multimer. doi:10.1101/2021.10.04.463034
1032 Fink S, Turnbull K, Desai A, Campbell CS. 2017. An engineered minimal chromosomal passenger
1033 complex reveals a role for INCENP/Sli15 spindle association in chromosome biorientation. *J Cell*
1034 *Biol* **216**:911–923. doi:10.1083/JCB.201609123
1035 Fischböck-Halwachs J, Singh S, Potocnjak M, Hagemann G, Solis-Mezarino V, Woike S, Ghodgaonkar-
1036 Steger M, Weissmann F, Gallego LD, Rojas J, Andreani J, Köhler A, Herzog F. 2019. The COMA
1037 complex interacts with Cse4 and positions Sli15/Ipl1 at the budding yeast inner kinetochore.
1038 *Elife* **8**. doi:10.7554/ELIFE.42879
1039 Foltz DR, Jansen LET, Black BE, Bailey AO, Yates JR, Cleveland DW. 2006. The human CENP-A
1040 centromeric nucleosome-associated complex. *Nat Cell Biol* **8**. doi:10.1038/ncb1397
1041 García-Rodríguez LJ, Kasciukovic T, Denninger V, Tanaka TU. 2019. Aurora B-INCENP Localization at
1042 Centromeres/Inner Kinetochores Is Required for Chromosome Bi-orientation in Budding Yeast.
1043 *Current Biology* **29**:1536-1544.e4. doi:10.1016/J.CUB.2019.03.051
1044 Gassmann R, Carvalho A, Henzing AJ, Ruchaud S, Hudson DF, Honda R, Nigg EA, Gerloff DL, Earnshaw
1045 WC. 2004. Borealin: a novel chromosomal passenger required for stability of the bipolar mitotic
1046 spindle. *Journal of Cell Biology* **166**. doi:10.1083/jcb.200404001
1047 Graham M, Combe C, Kolbowski L, Rappsilber J. 2019. xiView: A common platform for the
1048 downstream analysis of Crosslinking Mass Spectrometry data. *bioRxiv* 561829.
1049 doi:10.1101/561829
1050 Gruneberg U, Neef R, Honda R, Nigg EA, Barr FA. 2004. Relocation of Aurora B from centromeres to
1051 the central spindle at the metaphase to anaphase transition requires MKlp2. *J Cell Biol*
1052 **166**:167–172. doi:10.1083/JCB.200403084
1053 Hadders MA, Hindriksen S, Truong MA, Mhaskar AN, Pepijn Wopken J, Vromans MJM, Lens SMA.
1054 2020. Untangling the contribution of Haspin and Bub1 to Aurora B function during mitosis.
1055 *Journal of Cell Biology* **219**. doi:10.1083/JCB.201907087/133700
1056 Hayashi H, Akiyoshi B. 2018. Degradation of cyclin B is critical for nuclear division in *Trypanosoma*
1057 *brucei*. *Biol Open*. doi:10.1242/bio.031609
1058 Hochegger H, Hégarat N, Pereira-Leal JB. 2012. Aurora at the pole and equator: overlapping
1059 functions of Aurora kinases in the mitotic spindle. *Open Biol* **3**. doi:10.1098/RSOB.120185
1060 Hooff JJ, Tromer E, Wijk LM, Snel B, Kops GJ. 2017. Evolutionary dynamics of the kinetochore
1061 network in eukaryotes as revealed by comparative genomics. *EMBO Rep* **18**.
1062 doi:10.15252/embr.201744102

1063 Hori T, Fukagawa T. 2012. Establishment of the vertebrate kinetochores. *Chromosome Research* **20**.
1064 doi:10.1007/s10577-012-9289-9
1065 Hu H, Yu Z, Liu Y, Wang T, Wei Y, Li Z. 2014. The Aurora B kinase in *Trypanosoma brucei* undergoes
1066 post-translational modifications and is targeted to various subcellular locations through binding
1067 to TbCPC1. *Mol Microbiol* **91**. doi:10.1111/mmi.12458
1068 Hümmer S, Mayer TU. 2009. Cdk1 Negatively Regulates Midzone Localization of the Mitotic Kinesin
1069 Mklp2 and the Chromosomal Passenger Complex. *Current Biology* **19**:607–612.
1070 doi:10.1016/J.CUB.2009.02.046
1071 Integrating Neglected Tropical Diseases into Global Health and Development: Fourth World Health
1072 Organization Report on Neglected Tropical Diseases (WHO, 2017). 2017.
1073 Ishii M, Akiyoshi B. 2020. Characterization of unconventional kinetochore kinases KKT10/19 in
1074 *Trypanosoma brucei*. *J Cell Sci*. doi:10.1242/jcs.240978
1075 Izuta H, Ikeno M, Suzuki N, Tomonaga T, Nozaki N, Obuse C, Kisu Y, Goshima N, Nomura F, Nomura
1076 N, Yoda K. 2006. Comprehensive analysis of the ICEN (Interphase Centromere Complex)
1077 components enriched in the CENP-A chromatin of human cells. *Genes to Cells* **11**.
1078 doi:10.1111/j.1365-2443.2006.00969.x
1079 Je Van Hooff J, Tromer E, Van Wijk LM, Snel B, Geert &, Kops J. 2017. Evolutionary dynamics of the
1080 kinetochore network in eukaryotes as revealed by comparative genomics. *EMBO Rep* **18**:1559–
1081 1571. doi:10.15252/EMBR.201744102
1082 Jeyaprakash AA, Basquin C, Jayachandran U, Conti E. 2011. Structural Basis for the Recognition of
1083 Phosphorylated Histone H3 by the Survivin Subunit of the Chromosomal Passenger Complex.
1084 *Structure* **19**:1625–1634. doi:10.1016/J.STR.2011.09.002
1085 Jeyaprakash AA, Klein UR, Lindner D, Ebert J, Nigg EA, Conti E. 2007. Structure of a Survivin–
1086 Borealin–INCENP Core Complex Reveals How Chromosomal Passengers Travel Together. *Cell*
1087 **131**. doi:10.1016/j.cell.2007.07.045
1088 Jumper J, Evans R, Pritzel A, Green T, Figurnov M, Ronneberger O, Tunyasuvunakool K, Bates R, Žídek
1089 A, Potapenko A, Bridgland A, Meyer C, Kohl SAA, Ballard AJ, Cowie A, Romera-Paredes B,
1090 Nikolov S, Jain R, Adler J, Back T, Petersen S, Reiman D, Clancy E, Zielinski M, Steinegger M,
1091 Pacholska M, Berghammer T, Bodenstein S, Silver D, Vinyals O, Senior AW, Kavukcuoglu K, Kohli
1092 P, Hassabis D. 2021. Highly accurate protein structure prediction with AlphaFold. *Nature 2021*
1093 *596:7873* **596**:583–589. doi:10.1038/s41586-021-03819-2
1094 Kang JS, Cheeseman IM, Kallstrom G, Velmurugan S, Barnes G, Chan CSM. 2001. Functional
1095 cooperation of Dam1, Ipl1, and the inner centromere protein (INCENP)-related protein Sli15
1096 during chromosome segregation. *J Cell Biol* **155**:763–774. doi:10.1083/JCB.200105029
1097 Katoh K, Rozewicki J, Yamada KD. 2019. MAFFT online service: multiple sequence alignment,
1098 interactive sequence choice and visualization. *Brief Bioinform* **20**:1160–1166.
1099 doi:10.1093/BIB/BBX108
1100 Kawashima SA, Yamagishi Y, Honda T, Lshiguro KI, Watanabe Y. 2010. Phosphorylation of H2A by
1101 Bub1 prevents chromosomal instability through localizing shugoshin. *Science* **330**:172–177
1102 Kelly AE, Ghenoiu C, Xue JZ, Zierhut C, Kimura H, Funabiki H. 2010. Survivin reads phosphorylated
1103 histone H3 threonine 3 to activate the mitotic kinase Aurora B. *Science* **330**:235–239.
1104 doi:10.1126/SCIENCE.1189505
1105 Kelly S, Reed J, Kramer S, Ellis L, Webb H, Sunter J, Salje J, Marinsek N, Gull K, Wickstead B,
1106 Carrington M. 2007. Functional genomics in *Trypanosoma brucei*: A collection of vectors for the
1107 expression of tagged proteins from endogenous and ectopic gene loci. *Mol Biochem Parasitol*
1108 **154**. doi:10.1016/j.molbiopara.2007.03.012
1109 Kitagawa M, Fung SYS, Hameed UFS, Goto H, Inagaki M, Lee SH. 2014. Cdk1 coordinates timely
1110 activation of MKlp2 kinesin with relocation of the chromosome passenger complex for
1111 cytokinesis. *Cell Rep* **7**:166–179. doi:10.1016/J.CELREP.2014.02.034

1112 Klein UR, Nigg EA, Gruneberg U. 2006. Centromere targeting of the chromosomal passenger complex
1113 requires a ternary subcomplex of Borealin, Survivin, and the N-terminal domain of INCENP. *Mol*
1114 *Biol Cell* **17**:2547–2558. doi:10.1091/MBC.E05-12-1133
1115 Komaki S, Tromer EC, De Jaeger G, De Winne N, Heese M, Schnittger A. 2022. Molecular
1116 convergence by differential domain acquisition is a hallmark of chromosomal passenger
1117 complex evolution. *Proc Natl Acad Sci U S A* **119**. doi:10.1073/PNAS.2200108119/-
1118 /DCSUPPLEMENTAL
1119 Krenn V, Musacchio A. 2015. The Aurora B Kinase in Chromosome Bi-Orientation and Spindle
1120 Checkpoint Signaling. *Front Oncol* **5**. doi:10.3389/FONC.2015.00225
1121 Landeira D, Navarro M. 2007. Nuclear repositioning of the VSG promoter during developmental
1122 silencing in *Trypanosoma brucei*. *Journal of Cell Biology* **176**. doi:10.1083/jcb.200607174
1123 Leitner A, Reischl R, Walzthoeni T, Herzog F, Bohn S, Förster F, Aebersold R. 2012. Expanding the
1124 chemical cross-linking toolbox by the use of multiple proteases and enrichment by size
1125 exclusion chromatography. *Mol Cell Proteomics* **11**. doi:10.1074/MCP.M111.014126
1126 Li Z. 2012. Regulation of the Cell Division Cycle in *Trypanosoma brucei*. *Eukaryot Cell* **11**:1180.
1127 doi:10.1128/EC.00145-12
1128 Li Z, Lee JH, Chu F, Burlingame AL, Günzl A, Wang CC. 2008. Identification of a Novel Chromosomal
1129 Passenger Complex and Its Unique Localization during Cytokinesis in *Trypanosoma brucei*. *PLoS*
1130 *One* **3**. doi:10.1371/journal.pone.0002354
1131 Liang C, Zhang Z, Chen Q, Yan H, Zhang M, Zhou L, Xu J, Lu W, Wang F. 2020. Centromere-localized
1132 Aurora B kinase is required for the fidelity of chromosome segregation. *J Cell Biol* **219**.
1133 doi:10.1083/JCB.201907092
1134 Llauró A, Hayashi H, Bailey ME, Wilson A, Ludzia P, Asbury CL, Akiyoshi B. 2018. The kinetoplastid
1135 kinetochore protein KKT4 is an unconventional microtubule tip–coupling protein. *Journal of Cell*
1136 *Biology* **217**. doi:10.1083/jcb.201711181
1137 Lowell JE, Cross GAM. 2004. A variant histone H3 is enriched at telomeres in *Trypanosoma brucei*. *J*
1138 *Cell Sci* **117**:5937–5947. doi:10.1242/JCS.01515
1139 Ludzia P, Lowe ED, Marcianò G, Mohammed S, Redfield C, Akiyoshi B. 2021. Structural
1140 characterization of KKT4, an unconventional microtubule-binding kinetochore protein.
1141 *Structure* **29**:1014-1028.e8. doi:10.1016/J.STR.2021.04.004
1142 Mackay AM, Eckley DM, Chue C, Earnshaw WC. 1993. Molecular analysis of the INCENPs (inner
1143 centromere proteins): separate domains are required for association with microtubules during
1144 interphase and with the central spindle during anaphase. *J Cell Biol* **123**:373–385.
1145 doi:10.1083/JCB.123.2.373
1146 Maddox PS, Corbett KD, Desai A. 2012. Structure, assembly and reading of centromeric chromatin.
1147 *Curr Opin Genet Dev* **22**. doi:10.1016/j.gde.2011.11.005
1148 Marchetti MA, Tschudi C, Kwon H, Wolin SL, Ullu E. 2000. Import of proteins into the trypanosome
1149 nucleus and their distribution at karyokinesis. *J Cell Sci* **113 (Pt 5)**:899–906.
1150 doi:10.1242/JCS.113.5.899
1151 Marcianò G, Ishii M, Nerusheva OO, Akiyoshi B. 2021. Kinetoplastid kinetochore proteins KKT2 and
1152 KKT3 have unique centromere localization domains. *J Cell Biol* **220**. doi:10.1083/JCB.202101022
1153 Meraldi P, McAinsh AD, Rheinbay E, Sorger PK. 2006. Phylogenetic and structural analysis of
1154 centromeric DNA and kinetochore proteins. *Genome Biol* **7**:1–21. doi:10.1186/GB-2006-7-3-
1155 R23/FIGURES/11
1156 Mirdita M, Schütze K, Moriwaki Y, Heo L, Ovchinnikov S, Steinegger M. 2022. ColabFold: making
1157 protein folding accessible to all. *Nature Methods 2022 19:6* **19**:679–682. doi:10.1038/s41592-
1158 022-01488-1
1159 Nakajima Y, Cormier A, Tyers RG, Pigula A, Peng Y, Drubin DG, Barnes G. 2011. Ipl1/Aurora-
1160 dependent phosphorylation of Sli15/INCENP regulates CPC-spindle interaction to ensure
1161 proper microtubule dynamics. *J Cell Biol* **194**:137–153. doi:10.1083/JCB.201009137

1162 Nerusheva OO, Akiyoshi B. 2016. Divergent polo box domains underpin the unique kinetoplastid
1163 kinetochore. *Open Biol* **6**. doi:10.1098/rsob.150206
1164 Nerusheva OO, Ludzia P, Akiyoshi B. 2019. Identification of four unconventional kinetoplastid
1165 kinetochore proteins KKT22–25 in *Trypanosoma brucei*. *Open Biol* **9**. doi:10.1098/rsob.190236
1166 Noujaim M, Bechstedt S, Wieczorek M, Brouhard GJ. 2014. Microtubules accelerate the kinase
1167 activity of Aurora-B by a reduction in dimensionality. *PLoS One* **9**.
1168 doi:10.1371/JOURNAL.PONE.0086786
1169 Okada M, Cheeseman IM, Hori T, Okawa K, McLeod IX, Yates JR, Desai A, Fukagawa T. 2006. The
1170 CENP-H–I complex is required for the efficient incorporation of newly synthesized CENP-A into
1171 centromeres. *Nat Cell Biol* **8**. doi:10.1038/ncb1396
1172 Okada Y, Hirokawa N. 1999. A processive single-headed motor: Kinesin superfamily protein KIF1A.
1173 *Science (1979)* **283**:1152–1157. doi:10.1126/SCIENCE.283.5405.1152
1174 Perez-Riverol Y, Csordas A, Bai J, Bernal-Llinares M, Hewapathirana S, Kundu DJ, Inuganti A, Griss J,
1175 Mayer G, Eisenacher M, Pérez E, Uszkoreit J, Pfeuffer J, Sachsenberg T, Yilmaz Ş, Tiwary S, Cox J,
1176 Audain E, Walzer M, Jarnuczak AF, Ternent T, Brazma A, Vizcaíno JA. 2019. The PRIDE database
1177 and related tools and resources in 2019: improving support for quantification data. *Nucleic*
1178 *Acids Res* **47**:D442–D450. doi:10.1093/NAR/GKY1106
1179 Rice S, Lin AW, Safer D, Hart CL, Naber N, Carragher BO, Cain SM, Pechatnikova E, Wilson-Kubalek
1180 EM, Whittaker M, Pate E, Cooke R, Taylor EW, Milligan RA, Vale RD. 1999. A structural change
1181 in the kinesin motor protein that drives motility. *Nature 1999 402:6763* **402**:778–784.
1182 doi:10.1038/45483
1183 Romano A, Guse A, Krascenicova I, Schnabel H, Schnabel R, Glotzer M. 2003. CSC-1: a subunit of the
1184 Aurora B kinase complex that binds to the survivin-like protein BIR-1 and the incenp-like
1185 protein ICP-1. *Journal of Cell Biology* **161**. doi:10.1083/jcb.200207117
1186 Saldivia M, Fang E, Ma X, Myburgh E, Carnielli JBT, Bower-Lepts C, Brown E, Ritchie R,
1187 Lakshminarayana SB, Chen Y-L, Patra D, Ornelas E, Koh HXY, Williams SL, Supek F, Paape D,
1188 McCulloch R, Kaiser M, Barrett MP, Jiricek J, Diagana TT, Mottram JC, Rao SPS. 2020. Targeting
1189 the trypanosome kinetochore with CLK1 protein kinase inhibitors. *Nat Microbiol* **5**:1207–1216.
1190 doi:10.1038/s41564-020-0745-6
1191 Samejima K, Platani M, Wolny M, Ogawa H, Vargiu G, Knight PJ, Peckham M, Earnshaw WC. 2015.
1192 The Inner Centromere Protein (INCENP) Coil Is a Single α-Helix (SAH) Domain That Binds
1193 Directly to Microtubules and Is Important for Chromosome Passenger Complex (CPC)
1194 Localization and Function in Mitosis. *J Biol Chem* **290**:21460–21472.
1195 doi:10.1074/JBC.M115.645317
1196 Sampath SC, Ohi R, Leismann O, Salic A, Pozniakovski A, Funabiki H. 2004. The Chromosomal
1197 Passenger Complex Is Required for Chromatin-Induced Microtubule Stabilization and Spindle
1198 Assembly. *Cell* **118**. doi:10.1016/j.cell.2004.06.026
1199 Santaguida S, Musacchio A. 2009. The life and miracles of kinetochores. *EMBO J* **28**:2511–2531.
1200 doi:10.1038/EMBOJ.2009.173
1201 Schiffrin B, Radford SE, Brockwell DJ, Calabrese AN. 2020. PyXlinkViewer: A flexible tool for
1202 visualization of protein chemical crosslinking data within the PyMOL molecular graphics
1203 system. *Protein Sci* **29**:1851–1857. doi:10.1002/PRO.3902
1204 Schneider CA, Rasband WS, Eliceiri KW. 2012. NIH Image to ImageJ: 25 years of image analysis.
1205 *Nature Methods 2012 9:7* **9**:671–675. doi:10.1038/nmeth.2089
1206 Serena M, Bastos RN, Elliott PR, Barr FA. 2020. Molecular basis of MKLP2-dependent Aurora B
1207 transport from chromatin to the anaphase central spindle. *Journal of Cell Biology* **219**.
1208 doi:10.1083/JCB.201910059/151730
1209 Siegel TN, Hekstra DR, Cross GAM. 2008. Analysis of the *Trypanosoma brucei* cell cycle by
1210 quantitative DAPI imaging. *Mol Biochem Parasitol* **160**. doi:10.1016/j.molbiopara.2008.04.004

1211 Stuart K, Brun R, Croft S, Fairlamb A, Gürtler RE, McKerrow J, Reed S, Tarleton R. 2008.
1212 Kinetoplastids: related protozoan pathogens, different diseases. *Journal of Clinical Investigation*
1213 **118**. doi:10.1172/JCI33945
1214 Trivedi P, Stukenberg PT. 2016. A centromere-signaling network underlies the coordination among
1215 mitotic events. *Trends Biochem Sci* **41**:160. doi:10.1016/J.TIBS.2015.11.002
1216 Tromer EC, van Hooff JJE, Kops GJPL, Snel B. 2019. Mosaic origin of the eukaryotic kinetochore. *Proc*
1217 *Natl Acad Sci U S A* **116**:12873–12882.
1218 doi:10.1073/PNAS.1821945116/SUPPL_FILE/PNAS.1821945116.SD05.XLSX
1219 Tsukahara T, Tanno Y, Watanabe Y. 2010. Phosphorylation of the CPC by Cdk1 promotes
1220 chromosome bi-orientation. *Nature 2010 467:7316* **467**:719–723. doi:10.1038/nature09390
1221 Tu X, Kumar P, Li Z, Wang CC. 2006. An Aurora Kinase Homologue Is Involved in Regulating Both
1222 Mitosis and Cytokinesis in *Trypanosoma brucei*. *Journal of Biological Chemistry* **281**.
1223 doi:10.1074/jbc.M511504200
1224 Unnikrishnan A, Akiyoshi B, Biggins S, Tsukiyama T. 2012. An Efficient Purification System for Native
1225 Minichromosome from *Saccharomyces cerevisiae*. doi:10.1007/978-1-61779-477-3_8
1226 Vader G, Kauw JJW, Medema RH, Lens SMA. 2006. Survivin mediates targeting of the chromosomal
1227 passenger complex to the centromere and midbody. *EMBO Rep* **7**.
1228 doi:10.1038/sj.embor.7400562
1229 van der Horst A, Vromans MJM, Bouwman K, van der Waal MS, Hadders MA, Lens SMA. 2015. Inter-
1230 domain Cooperation in INCENP Promotes Aurora B Relocation from Centromeres to
1231 Microtubules. *Cell Rep* **12**:380–387. doi:10.1016/J.CELREP.2015.06.038
1232 Van Der Lee R, Buljan M, Lang B, Weatheritt RJ, Daughdrill GW, Dunker AK, Fuxreiter M, Gough J,
1233 Gsponer J, Jones DT, Kim PM, Kriwacki RW, Oldfield CJ, Pappu R V., Tompa P, Uversky VN,
1234 Wright PE, Babu MM. 2014. Classification of intrinsically disordered regions and proteins. *Chem*
1235 *Rev* **114**:6589–6631. doi:10.1021/CR400525M/ASSET/IMAGES/LARGE/CR-2013-
1236 00525M_0006.JPEG
1237 Wang F, Dai J, Daum JR, Niedzialkowska E, Banerjee B, Stukenberg PT, Gorbsky GJ, Higgins JMG.
1238 2010. Histone H3 Thr-3 phosphorylation by Haspin positions Aurora B at centromeres in
1239 mitosis. *Science* **330**:231–235. doi:10.1126/SCIENCE.1189435
1240 Waterhouse AM, Procter JB, Martin DMA, Clamp M, Barton GJ. 2009. Jalview Version 2--a multiple
1241 sequence alignment editor and analysis workbench. *Bioinformatics* **25**:1189–1191.
1242 doi:10.1093/BIOINFORMATICS/BTP033
1243 Westhorpe FG, Straight AF. 2013. Functions of the centromere and kinetochore in chromosome
1244 segregation. *Curr Opin Cell Biol* **25**. doi:10.1016/j.ceb.2013.02.001
1245 Wheatley SP, Carvalho A, Vagnarelli P, Earnshaw WC. 2001. INCENP is required for proper targeting
1246 of Survivin to the centromeres and the anaphase spindle during mitosis. *Current Biology* **11**.
1247 doi:10.1016/S0960-9822(01)00238-X
1248 Wheelock MS, Wynne DJ, Tseng BS, Funabiki H. 2017. Dual recognition of chromatin and
1249 microtubules by INCENP is important for mitotic progression. *J Cell Biol* **216**:925–941.
1250 doi:10.1083/JCB.201609061
1251 Wickstead B, Gull K. 2006. A “Holistic” Kinesin Phylogeny Reveals New Kinesin Families and Predicts
1252 Protein Functions. *Mol Biol Cell* **17**:1734–1743. doi:10.1091/mbc.E05-11-1090
1253 Woods A, Sherwin T, Sasse R, MacRae TH, Baines AJ, Gull K. 1989. Definition of individual
1254 components within the cytoskeleton of *Trypanosoma brucei* by a library of monoclonal
1255 antibodies. *J Cell Sci* **93**:491–500. doi:10.1242/JCS.93.3.491
1256 Woodward R, Gull K. 1990. Timing of nuclear and kinetoplast DNA replication and early
1257 morphological events in the cell cycle of *Trypanosoma brucei*. *J Cell Sci* **95**.
1258 doi:10.1242/jcs.95.1.49
1259 Yamagishi Y, Honda T, Tanno Y, Watanabe Y. 2010. Two histone marks establish the inner
1260 centromere and chromosome bi-orientation. *Science* **330**:239–243.
1261 doi:10.1126/SCIENCE.1194498

1262 Yoon HJ, Carbon J. 1999. Participation of Bir1p, a member of the inhibitor of apoptosis family, in
1263 yeast chromosome segregation events. *Proc Natl Acad Sci U S A* **96**:13208–13213.
1264 doi:10.1073/PNAS.96.23.13208
1265 Zimniak T, Fitz V, Zhou H, Lampert F, Opravil S, Mechtler K, Stolt-Bergner P, Westermann S. 2012.
1266 Spatiotemporal regulation of Ipl1/Aurora activity by direct Cdk1 phosphorylation. *Curr Biol*
1267 **22**:787–793. doi:10.1016/J.CUB.2012.03.007
1268

Figure 1

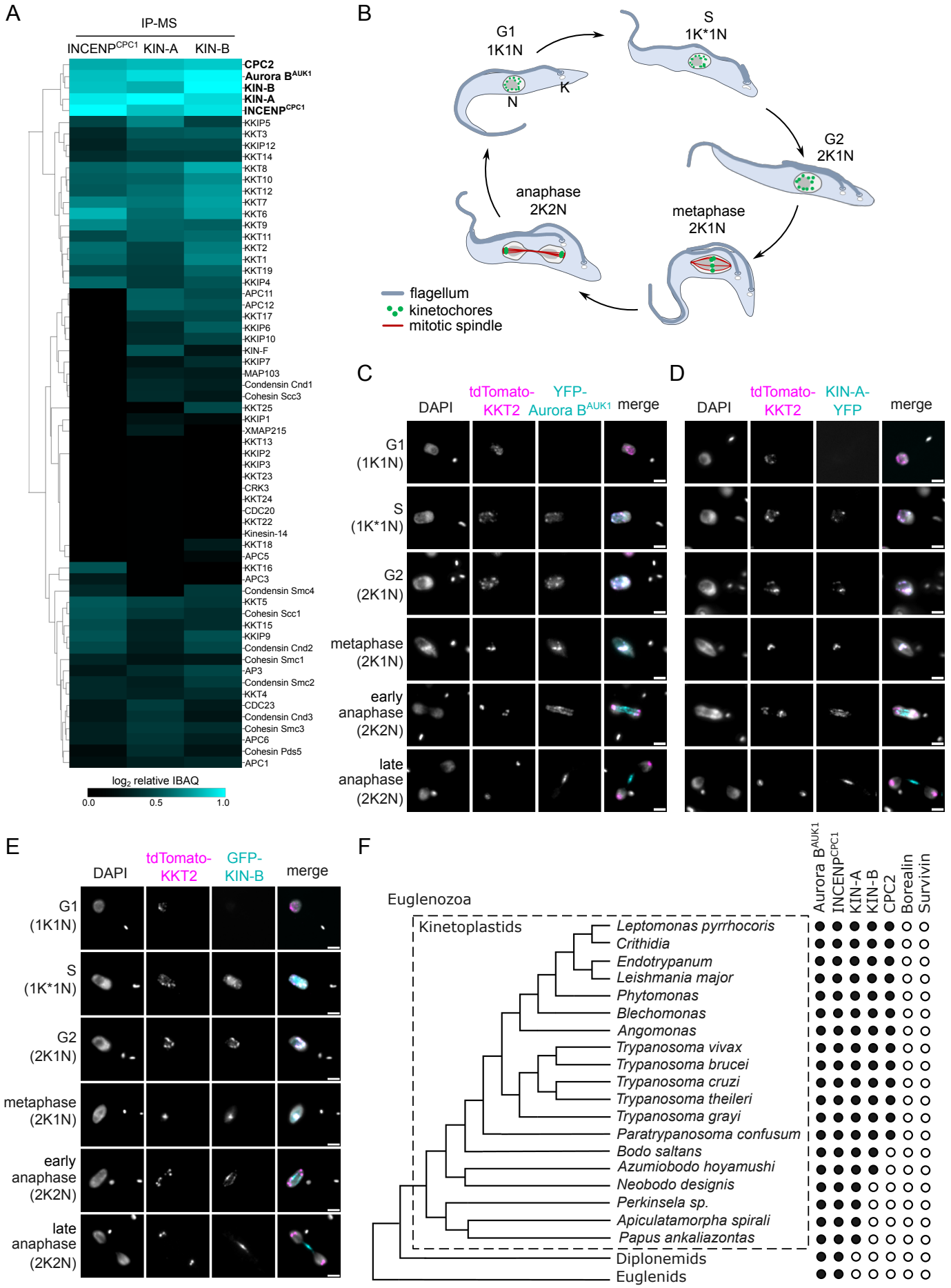
A
IP-MS
INCENP^CPC1
KIN-A
KIN-B
CPC2
Aurora B^AUK1
KIN-B
KIN-A
INCENP^CPC1
KKIP5
KKT3
KKIP12
KKT14
KKT8
KKT10
KKT12
KKT7
KKT6
KKT9
KKT11
KKT2
KKT1
KKT19
KKIP4
APC11
APC12
KKT17
KKIP6
KKIP10
KIN-F
KKIP7
MAP103
Condensin Cnd1
Cohesin Scc3
KKT25
KKIP1
XMAP215
KKT13
KKIP2
KKIP3
KKT23
CRK3
KKT24
CDC20
KKT22
Kinesin-14
KKT18
APC5
KKT16
APC3
Condensin Smc4
KKT5
Cohesin Scc1
KKT15
KKIP9
Condensin Cnd2
Cohesin Smc1
AP3
Condensin Smc2
KKT4
CDC23
Condensin Cnd3
Cohesin Smc3
APC6
Cohesin Pds5
APC1
log2 relative IBAQ
0.0
0.5
1.0
B
G1
1K1N
N
K
S
1K*1N
G2
2K1N
metaphase
2K1N
anaphase
2K2N
flagellum
kinetochores
mitotic spindle
C
DAPI
tdTomato-KKT2
YFP-Aurora B^AUK1
merge
G1 (1K1N)
S (1K*1N)
G2 (2K1N)
metaphase (2K1N)
early anaphase (2K2N)
late anaphase (2K2N)
D
DAPI
tdTomato-KKT2
KIN-A-YFP
merge
E
DAPI
tdTomato-KKT2
GFP-KIN-B
merge
G1 (1K1N)
S (1K*1N)
G2 (2K1N)
metaphase (2K1N)
early anaphase (2K2N)
late anaphase (2K2N)
F
Euglenozoa
Kinetoplastids
Leptomonas pyrrhocoris
Crithidia
Endotrypanum
Leishmania major
Phytomonas
Blechomonas
Angomonas
Trypanosoma vivax
Trypanosoma brucei
Trypanosoma cruzi
Trypanosoma theileri
Trypanosoma grayi
Paratrypanosoma confusum
Bodo saltans
Azumiobodo hoyamushi
Neobodo designis
Perkinsela sp.
Apiculatamorpha spirali
Papus ankaliazontas
Diplonemids
Euglenids
Aurora B^AUK1
INCENP^CPC1
KIN-A
KIN-B
CPC2
Borealin
Survivin

Figure 2

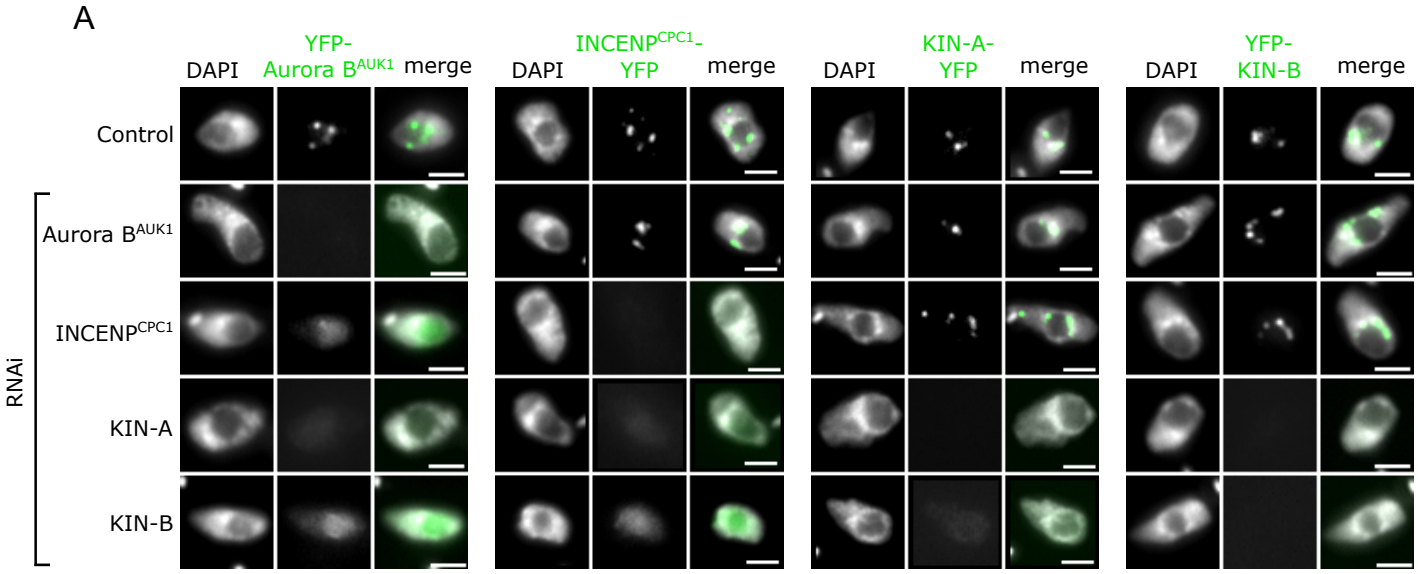
A
DAPI
YFP-Aurora B^AUK1
merge
INCENP^CPC1-YFP
KIN-A-YFP
YFP-KIN-B
Control
Aurora B^AUK1
INCENP^CPC1
KIN-A
KIN-B
RNAi

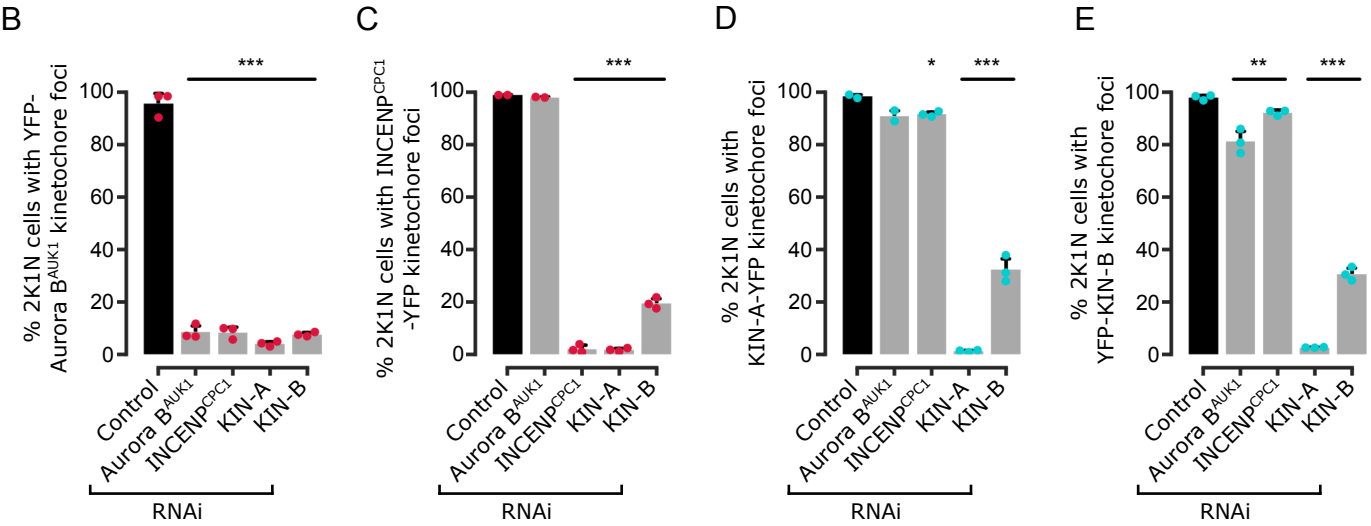
B
% 2K1N cells with YFP-Aurora B^AUK1 kinetochore foci
C
% 2K1N cells with INCENP^CPC1-YFP kinetochore foci
D
% 2K1N cells with KIN-A-YFP kinetochore foci
E
% 2K1N cells with YFP-KIN-B kinetochore foci
***
*
**
Control
Aurora B^AUK1
INCENP^CPC1
KIN-A
KIN-B
RNAi

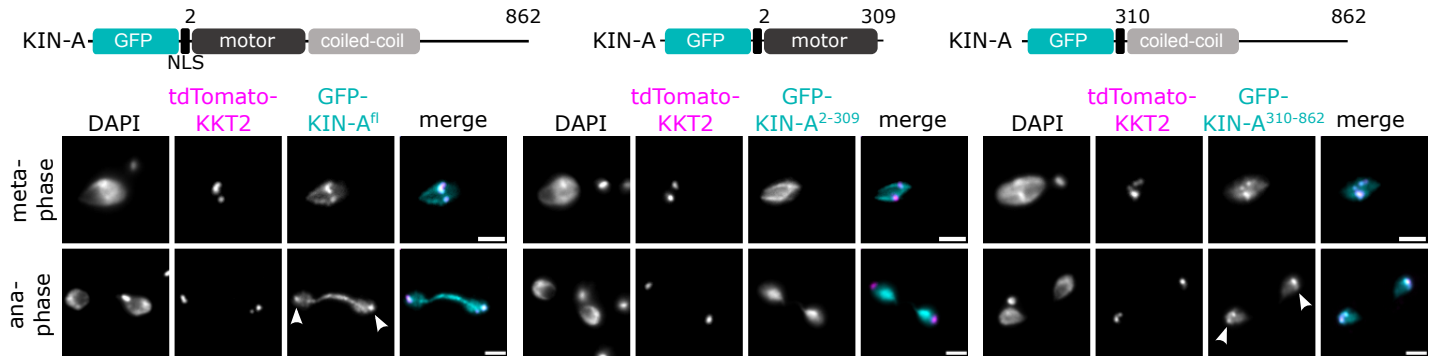
F
G
H
KIN-A-
GFP
NLS
motor
coiled-coil
2
862
309
310
DAPI
tdTomato-KKT2
GFP-KIN-A^fl
GFP-KIN-A^2-309
GFP-KIN-A^310-862
merge
meta-phase
ana-phase

Figure 3

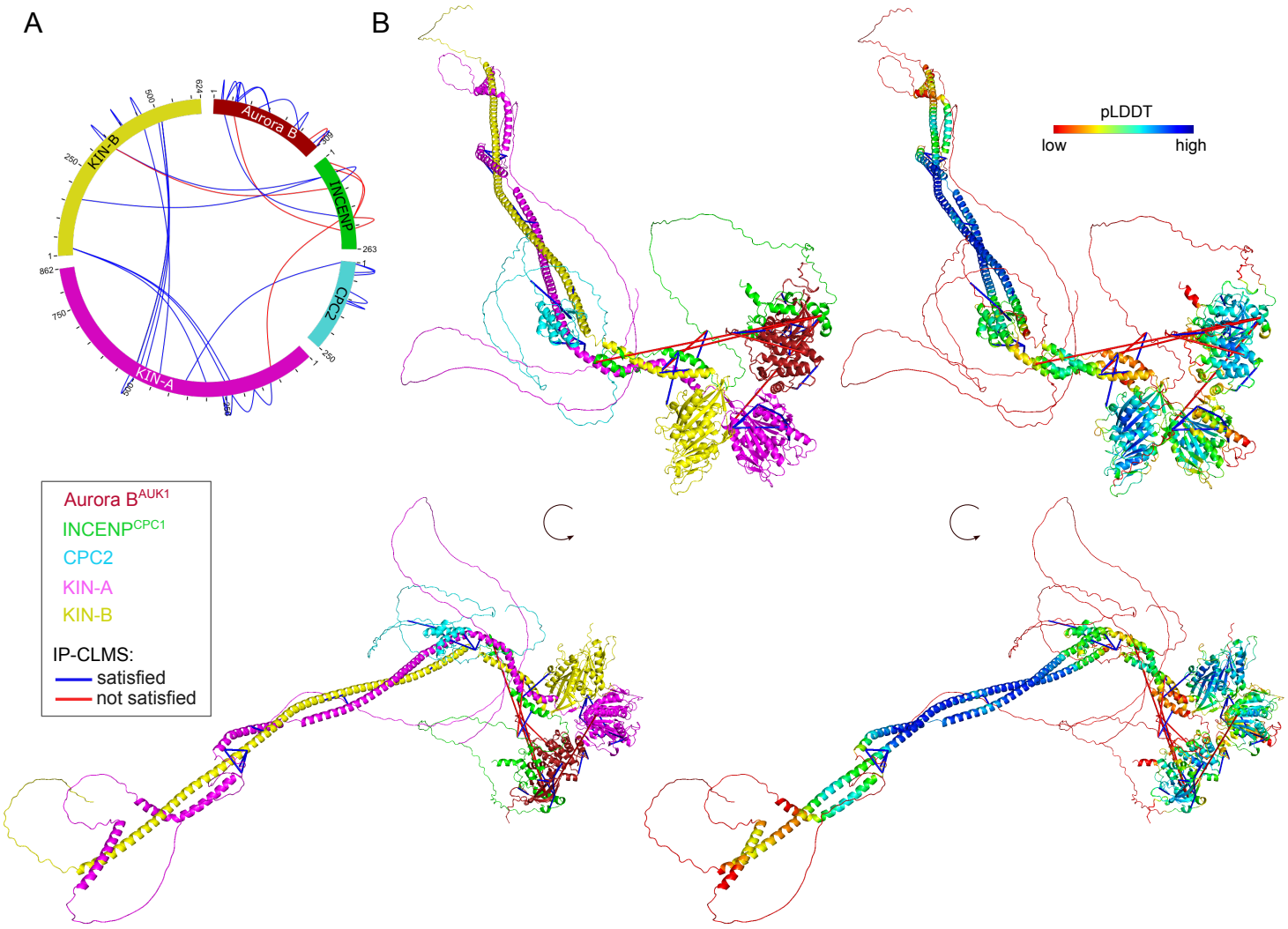
A
B
Aurora B
INCENP
CPC2
KIN-A
KIN-B
pLDDT
low
high
Aurora B^AUK1
INCENP^CPC1
CPC2
KIN-A
KIN-B
IP-CLMS:
satisfied
not satisfied

Figure 4

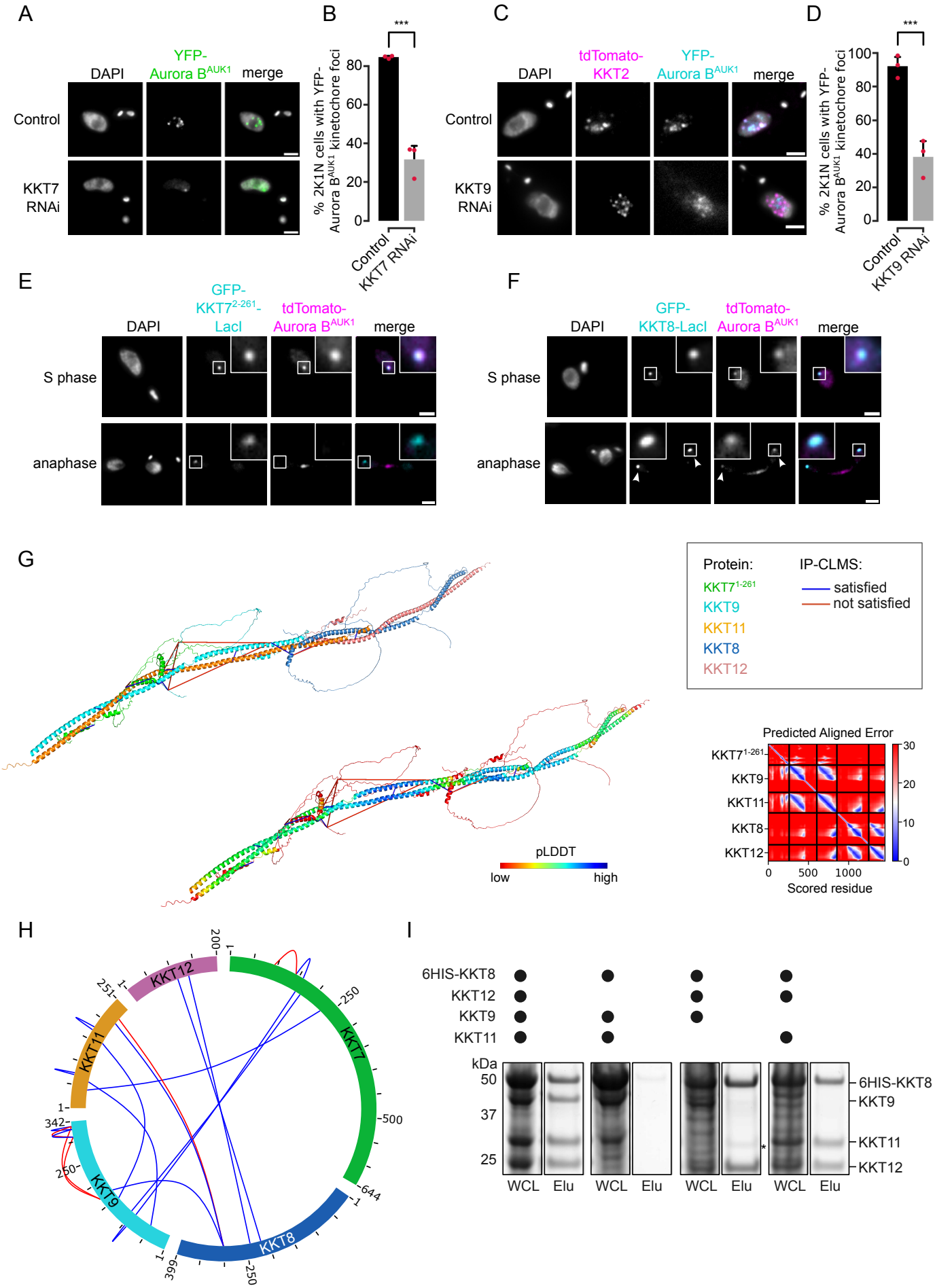

A
DAPI
YFP-Aurora B^AUK1
merge
Control
KKT7 RNAi
B
***
% 2K1N cells with YFP-Aurora B^AUK1 kinetochore foci
Control
KKT7 RNAi
C
DAPI
tdTomato-KKT2
YFP-Aurora B^AUK1
merge
Control
KKT9 RNAi
D
***
% 2K1N cells with YFP-Aurora B^AUK1 kinetochore foci
Control
KKT9 RNAi
E
DAPI
GFP-KKT7^2-261-LacI
tdTomato-Aurora B^AUK1
merge
S phase
anaphase
F
DAPI
GFP-KKT8-LacI
tdTomato-Aurora B^AUK1
merge
S phase
anaphase
G
Protein:
KKT7^1-261
KKT9
KKT11
KKT8
KKT12
IP-CLMS:
satisfied
not satisfied
pLDDT
low
high
Predicted Aligned Error
KKT7^1-261
KKT9
KKT11
KKT8
KKT12
Scored residue
H
KKT12
KKT7
KKT11
KKT9
KKT8
I
6HIS-KKT8
KKT12
KKT9
KKT11
kDa
WCL
Elu

Figure 5

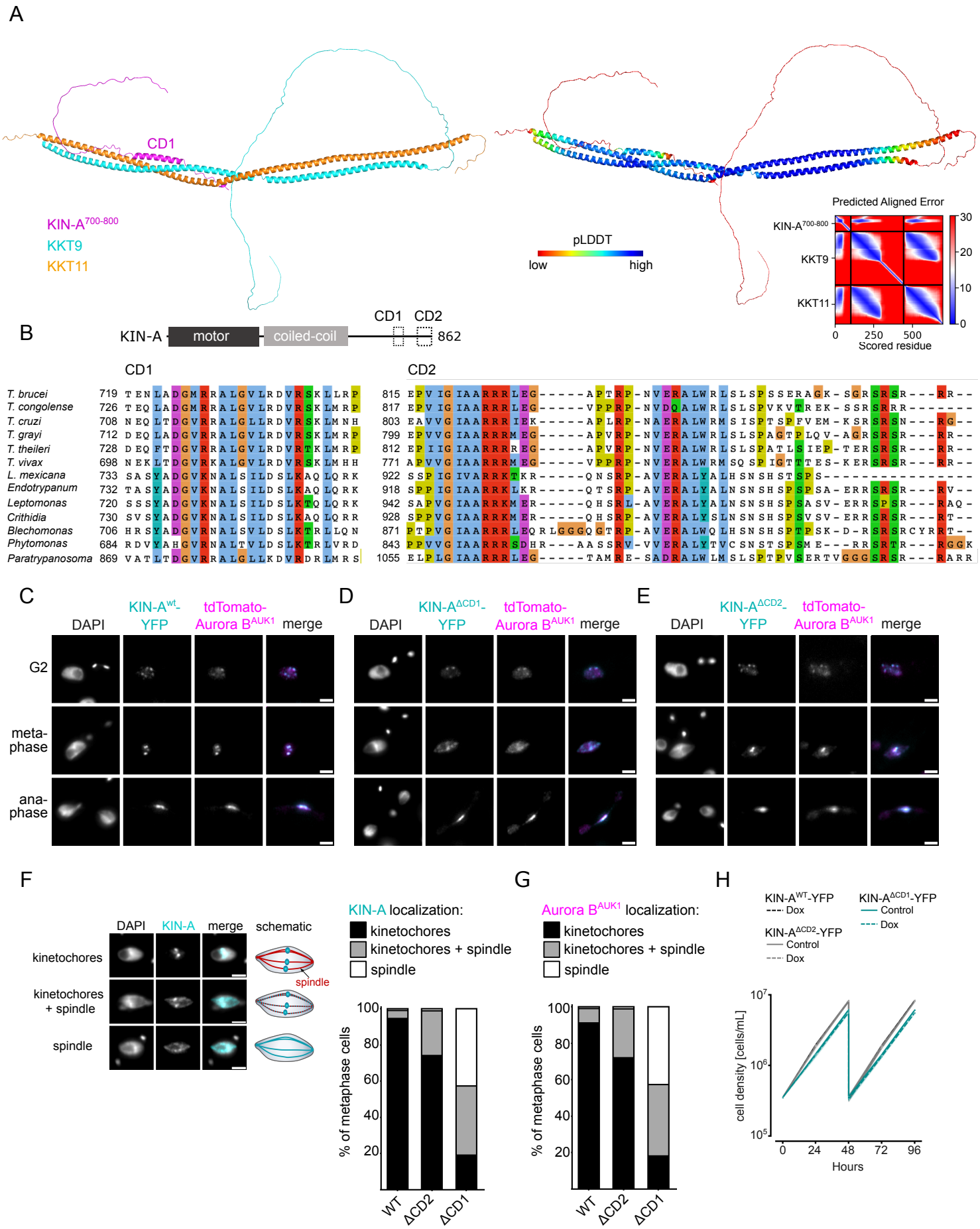
A
CD1
KIN-A700-800
KKT9
KKT11
pLDDT
low
high
Predicted Aligned Error
KIN-A700-800
KKT9
KKT11
Scored residue
B
KIN-A
motor
coiled-coil
CD1
CD2
862
CD1
CD2
T. brucei
T. congolense
T. cruzi
T. grayi
T. theileri
T. vivax
L. mexicana
Endotrypanum
Leptomonas
Crithidia
Blechomonas
Phytomonas
Paratrypanosoma
C
DAPI
KIN-Awt-YFP
tdTomato-Aurora BAUK1
merge
G2
meta-phase
ana-phase
D
KIN-AΔCD1-YFP
E
KIN-AΔCD2-YFP
F
DAPI
KIN-A
merge
schematic
kinetochores
kinetochores + spindle
spindle
KIN-A localization:
kinetochores
kinetochores + spindle
spindle
% of metaphase cells
WT
ΔCD2
ΔCD1
G
Aurora BAUK1 localization:
H
KIN-AWT-YFP
Dox
KIN-AΔCD1-YFP
Control
Dox
KIN-AΔCD2-YFP
Control
Dox
cell density [cells/mL]
Hours

Figure 6

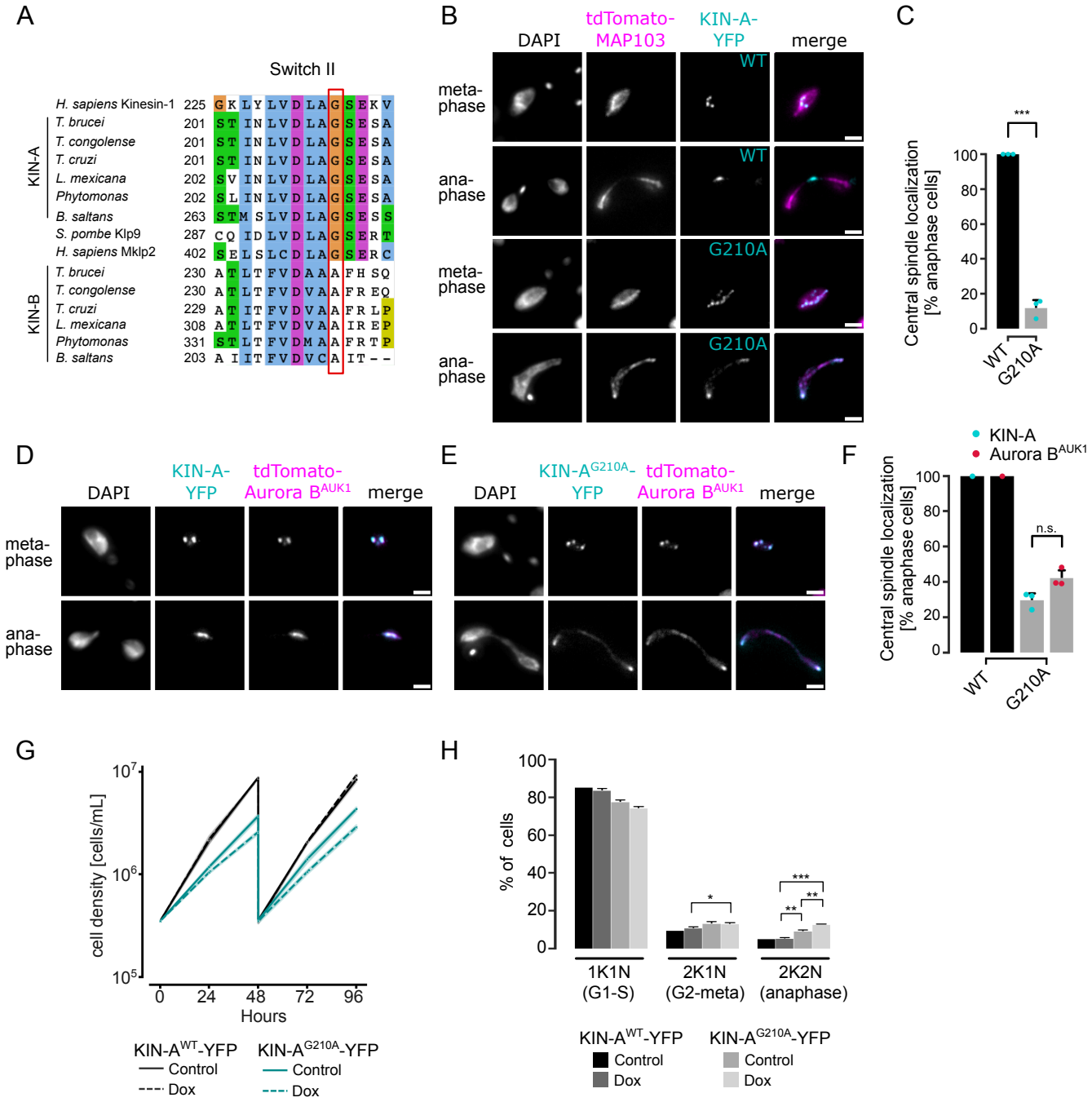
A
Switch II
H. sapiens Kinesin-1 225 G K L Y L V D L A G S E K V
KIN-A
T. brucei 201 S T I N L V D L A G S E S A
T. congolense 201 S T I N L V D L A G S E S A
T. cruzi 201 S T I N L V D L A G S E S A
L. mexicana 202 S V I N L V D L A G S E S A
Phytomonas 202 S L I N L V D L A G S E S A
B. saltans 263 S T M S L V D L A G S E S S
S. pombe Klp9 287 C Q I D L V D L A G S E R T
H. sapiens Mklp2 402 S E L S L C D L A G S E R C
KIN-B
T. brucei 230 A T L T F V D A A A F H S Q
T. congolense 230 A T L T F V D V A A F R E Q
T. cruzi 229 A T I T F V D V A A F R L P
L. mexicana 308 A T L T F V D V A A I R E P
Phytomonas 331 S T L T F V D M A A F R T P
B. saltans 203 A I I T F V D V C A I T - -
B
DAPI
tdTomato-MAP103
KIN-A-YFP
merge
meta-phase
ana-phase
meta-phase
ana-phase
WT
WT
G210A
G210A
C
Central spindle localization [% anaphase cells]
100
80
60
40
20
0
***
WT
G210A
D
DAPI
KIN-A-YFP
tdTomato-Aurora B^AUK1
merge
meta-phase
ana-phase
E
DAPI
KIN-A^G210A-YFP
tdTomato-Aurora B^AUK1
merge
F
KIN-A
Aurora B^AUK1
Central spindle localization [% anaphase cells]
100
80
60
40
20
0
n.s.
WT
G210A
G
cell density [cells/mL]
10^7
10^6
10^5
0
24
48
72
96
Hours
KIN-A^WT-YFP
Control
Dox
KIN-A^G210A-YFP
Control
Dox
H
% of cells
100
80
60
40
20
0
*
***
**
**
1K1N (G1-S)
2K1N (G2-meta)
2K2N (anaphase)
KIN-A^WT-YFP
Control
Dox
KIN-A^G210A-YFP
Control
Dox

Figure 7

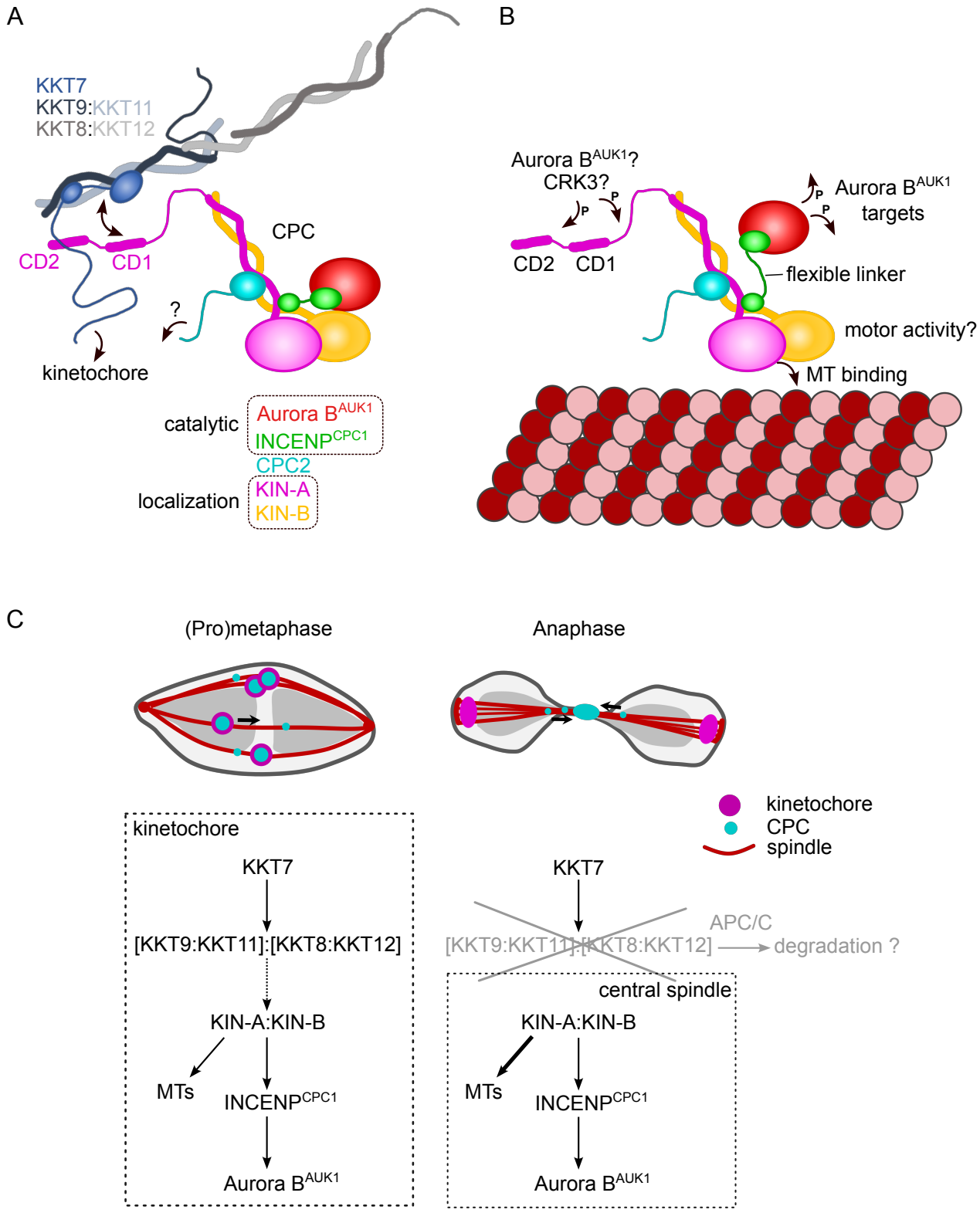
A
KKT7
KKT9:KKT11
KKT8:KKT12
CD2
CD1
CPC
?
kinetochore
catalytic
Aurora B^AUK1
INCENP^CPC1
CPC2
localization
KIN-A
KIN-B
B
Aurora B^AUK1?
CRK3?
P
P
CD2
CD1
Aurora B^AUK1
targets
P
P
flexible linker
motor activity?
MT binding
C
(Pro)metaphase
Anaphase
kinetochore
CPC
spindle
kinetochore
KKT7
[KKT9:KKT11]:[KKT8:KKT12]
KIN-A:KIN-B
MTs
INCENP^CPC1
Aurora B^AUK1
KKT7
APC/C
[KKT9:KKT11]:[KKT8:KKT12]
degradation ?
central spindle
KIN-A:KIN-B
MTs
INCENP^CPC1
Aurora B^AUK1

Figure S1

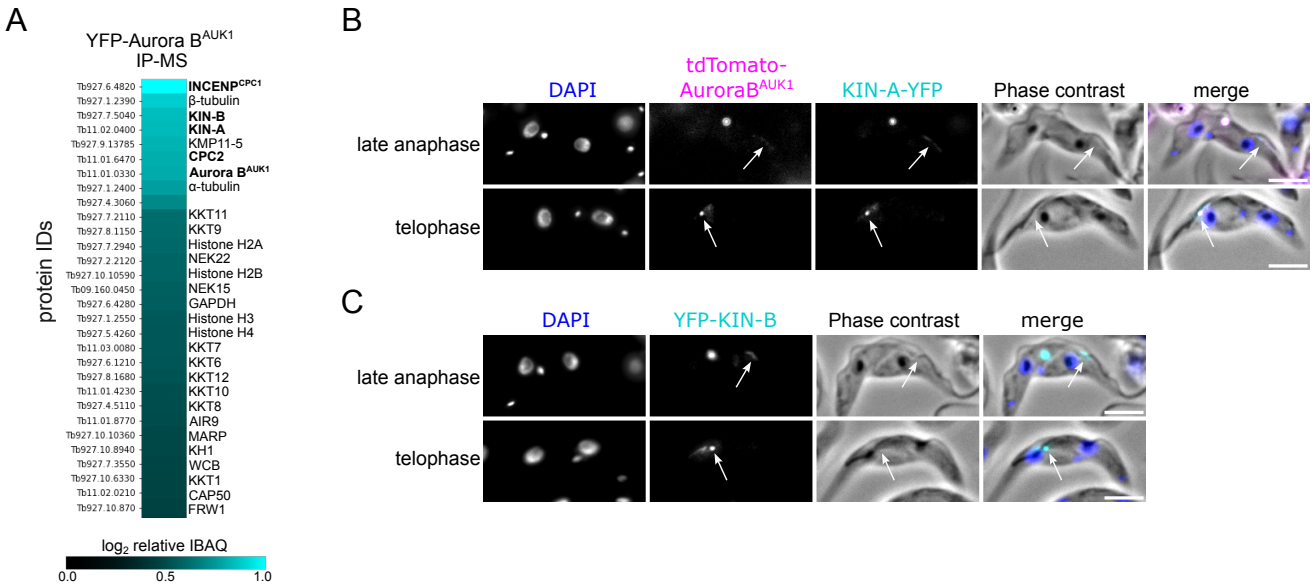
A
YFP-Aurora B^AUK1
IP-MS
protein IDs
Tb927.6.4820 INCENP^CPC1
Tb927.1.2390 β-tubulin
Tb927.7.5040 KIN-B
Tb11.02.0400 KIN-A
Tb927.9.13785 KMP11-5
Tb11.01.6470 CPC2
Tb11.01.0330 Aurora B^AUK1
Tb927.1.2400 α-tubulin
Tb927.4.3060
Tb927.7.2110 KKT11
Tb927.8.1150 KKT9
Tb927.7.2940 Histone H2A
Tb927.2.2120 NEK22
Tb927.10.10590 Histone H2B
Tb09.160.0450 NEK15
Tb927.6.4280 GAPDH
Tb927.1.2550 Histone H3
Tb927.5.4260 Histone H4
Tb11.03.0080 KKT7
Tb927.6.1210 KKT6
Tb927.8.1680 KKT12
Tb11.01.4230 KKT10
Tb927.4.5110 KKT8
Tb11.01.8770 AIR9
Tb927.10.10360 MARP
Tb927.10.8940 KH1
Tb927.7.3550 WCB
Tb927.10.6330 KKT1
Tb11.02.0210 CAP50
Tb927.10.870 FRW1
log2 relative IBAQ
0.0
0.5
1.0
B
DAPI
tdTomato-AuroraB^AUK1
KIN-A-YFP
Phase contrast
merge
late anaphase
telophase
C
DAPI
YFP-KIN-B
Phase contrast
merge
late anaphase
telophase

Figure S2

A

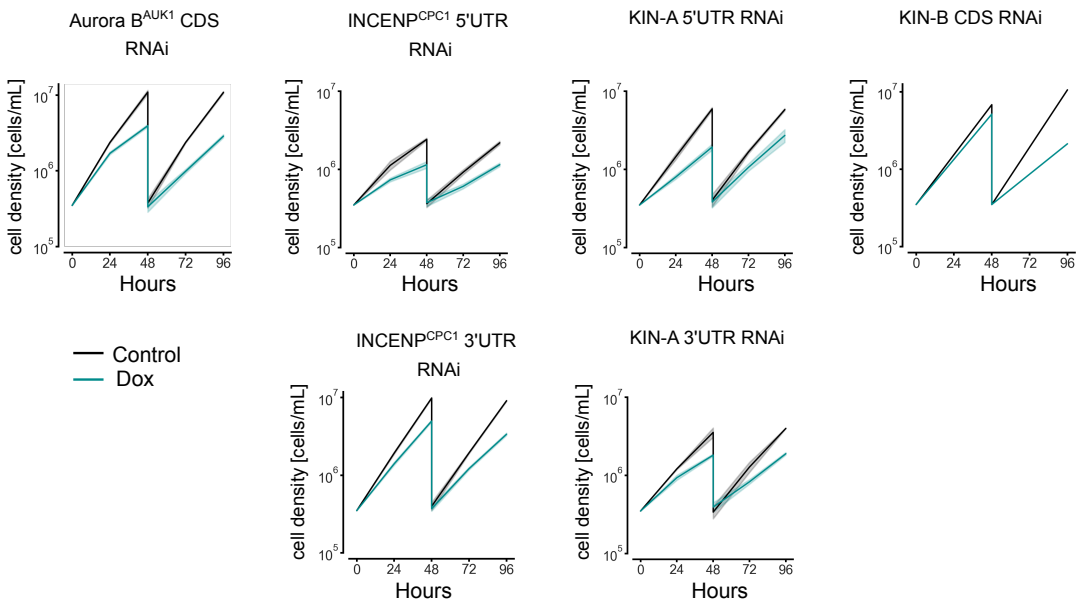

B

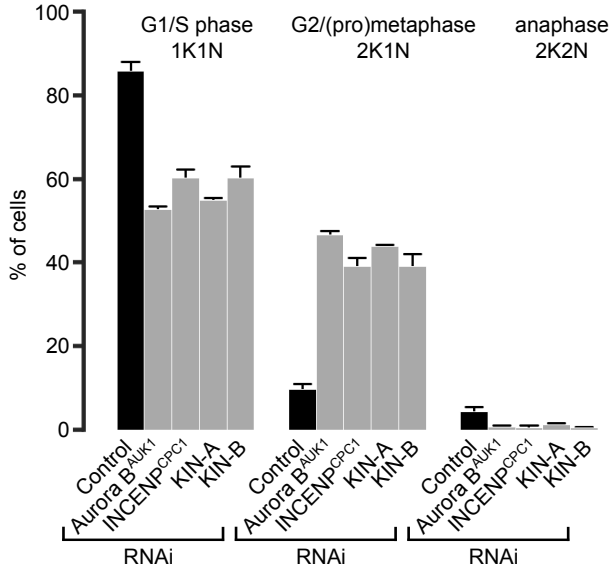

C

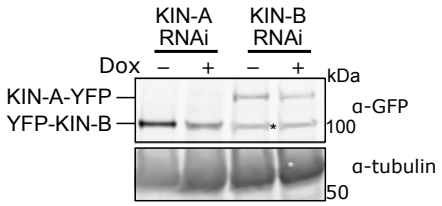

D

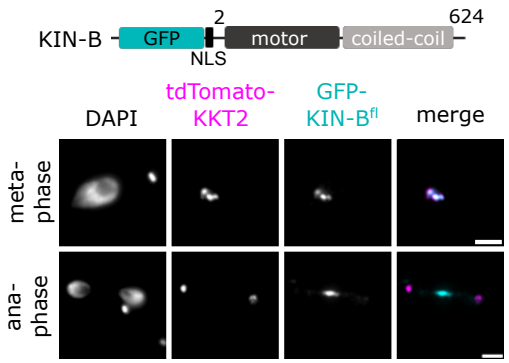

E

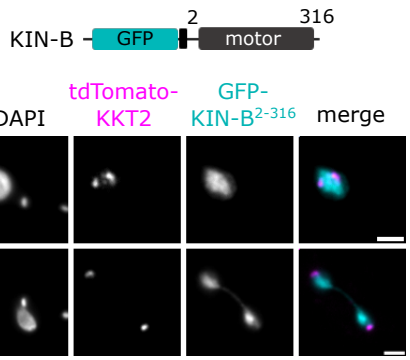

F

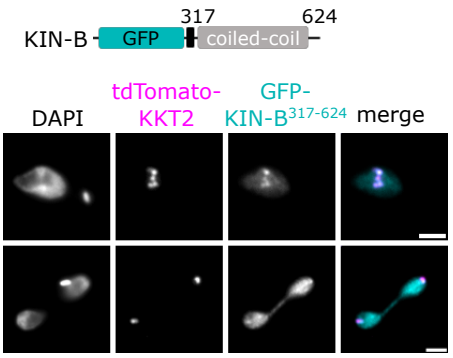

Figure S3

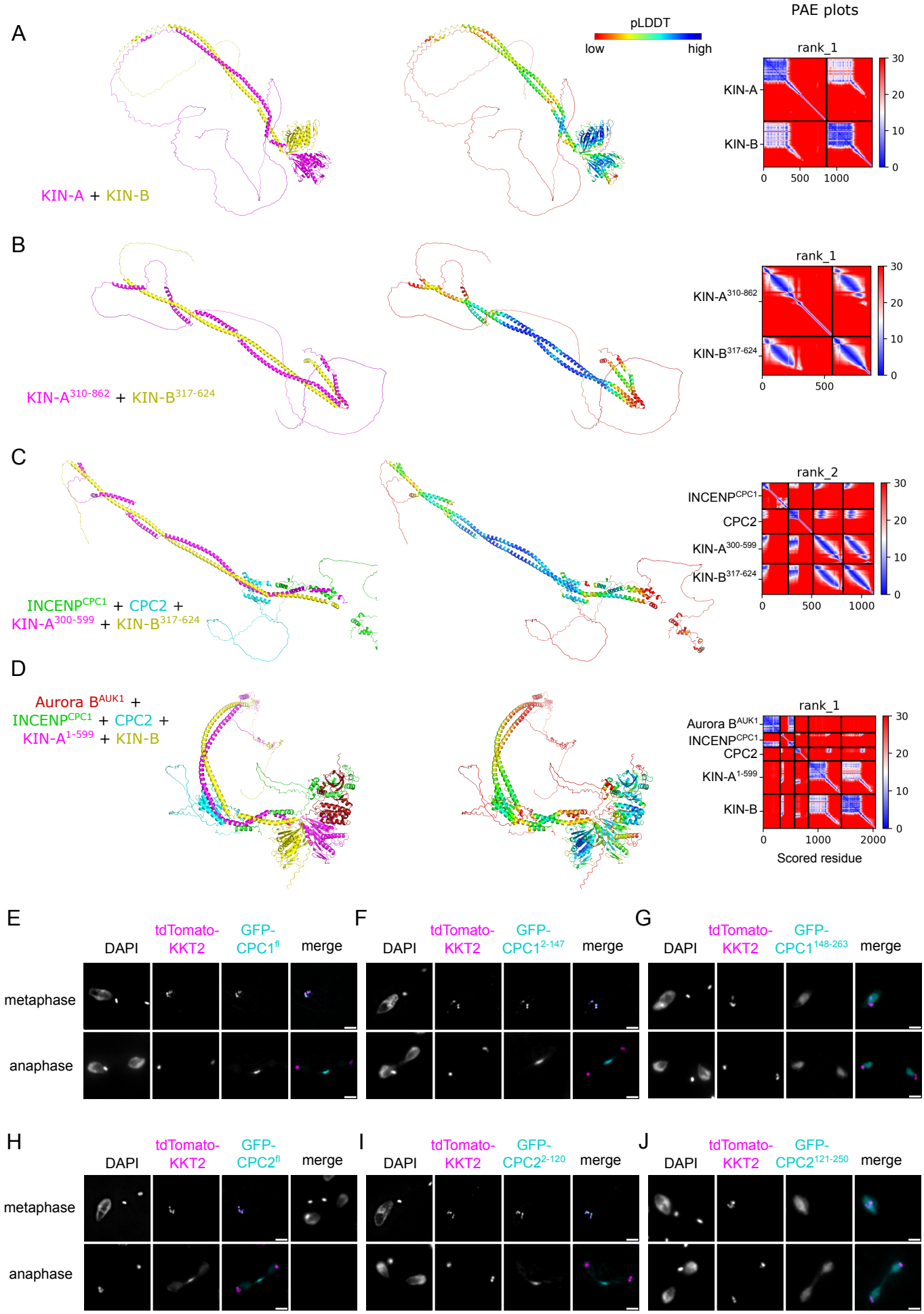
A
pLDDT
low
high
PAE plots
rank_1
KIN-A
KIN-B
KIN-A + KIN-B
B
rank_1
KIN-A310-862
KIN-B317-624
KIN-A310-862 + KIN-B317-624
C
rank_2
INCENPCPC1
CPC2
KIN-A300-599
KIN-B317-624
INCENPCPC1 + CPC2 +
KIN-A300-599 + KIN-B317-624
D
Aurora BAUK1 +
INCENPCPC1 + CPC2 +
KIN-A1-599 + KIN-B
rank_1
Aurora BAUK1
INCENPCPC1
CPC2
KIN-A1-599
KIN-B
Scored residue
E
DAPI
tdTomato-KKT2
GFP-CPC1fl
merge
metaphase
anaphase
F
GFP-CPC1 2-147
G
GFP-CPC1 148-263
H
GFP-CPC2fl
I
GFP-CPC2 2-120
J
GFP-CPC2 121-250

Figure S4 (i)

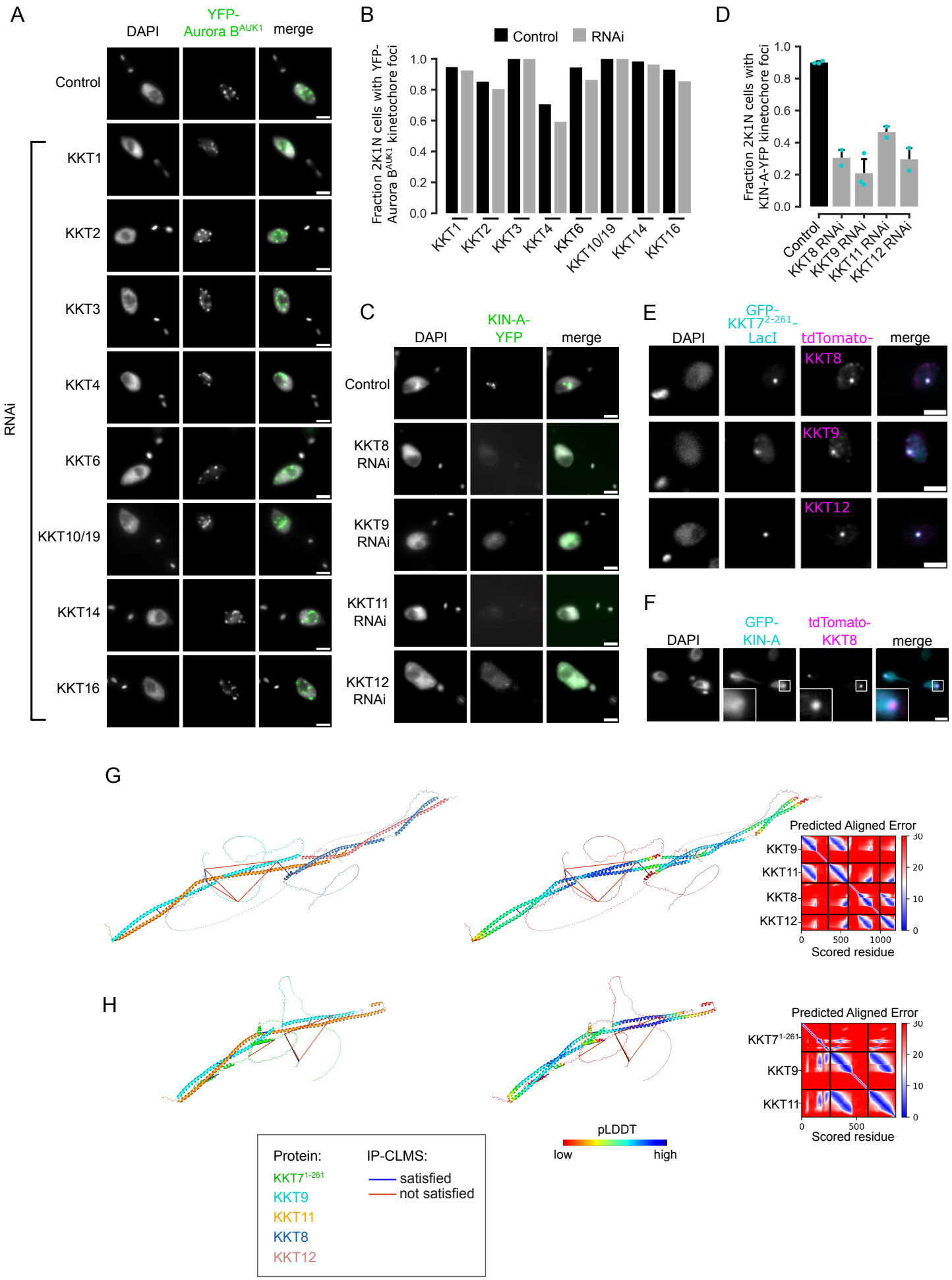
A
DAPI
YFP-Aurora B^AUK1
merge
Control
KKT1
KKT2
KKT3
KKT4
KKT6
KKT10/19
KKT14
KKT16
RNAi
B
Control
RNAi
Fraction 2K1N cells with YFP-Aurora B^AUK1 kinetochore foci
1.0
0.8
0.6
0.4
0.2
0.0
KKT1
KKT2
KKT3
KKT4
KKT6
KKT10/19
KKT14
KKT16
D
Fraction 2K1N cells with KIN-A-YFP kinetochore foci
Control
KKT8 RNAi
KKT9 RNAi
KKT11 RNAi
KKT12 RNAi
C
DAPI
KIN-A-YFP
merge
Control
KKT8 RNAi
KKT9 RNAi
KKT11 RNAi
KKT12 RNAi
E
DAPI
GFP-KKT7^2-261-LacI
tdTomato-
merge
KKT8
KKT9
KKT12
F
DAPI
GFP-KIN-A
tdTomato-KKT8
merge
G
Predicted Aligned Error
KKT9
KKT11
KKT8
KKT12
Scored residue
H
Predicted Aligned Error
KKT7^1-261
KKT9
KKT11
Scored residue
pLDDT
low
high
Protein:
KKT7^1-261
KKT9
KKT11
KKT8
KKT12
IP-CLMS:
satisfied
not satisfied

Figure S4 (ii)

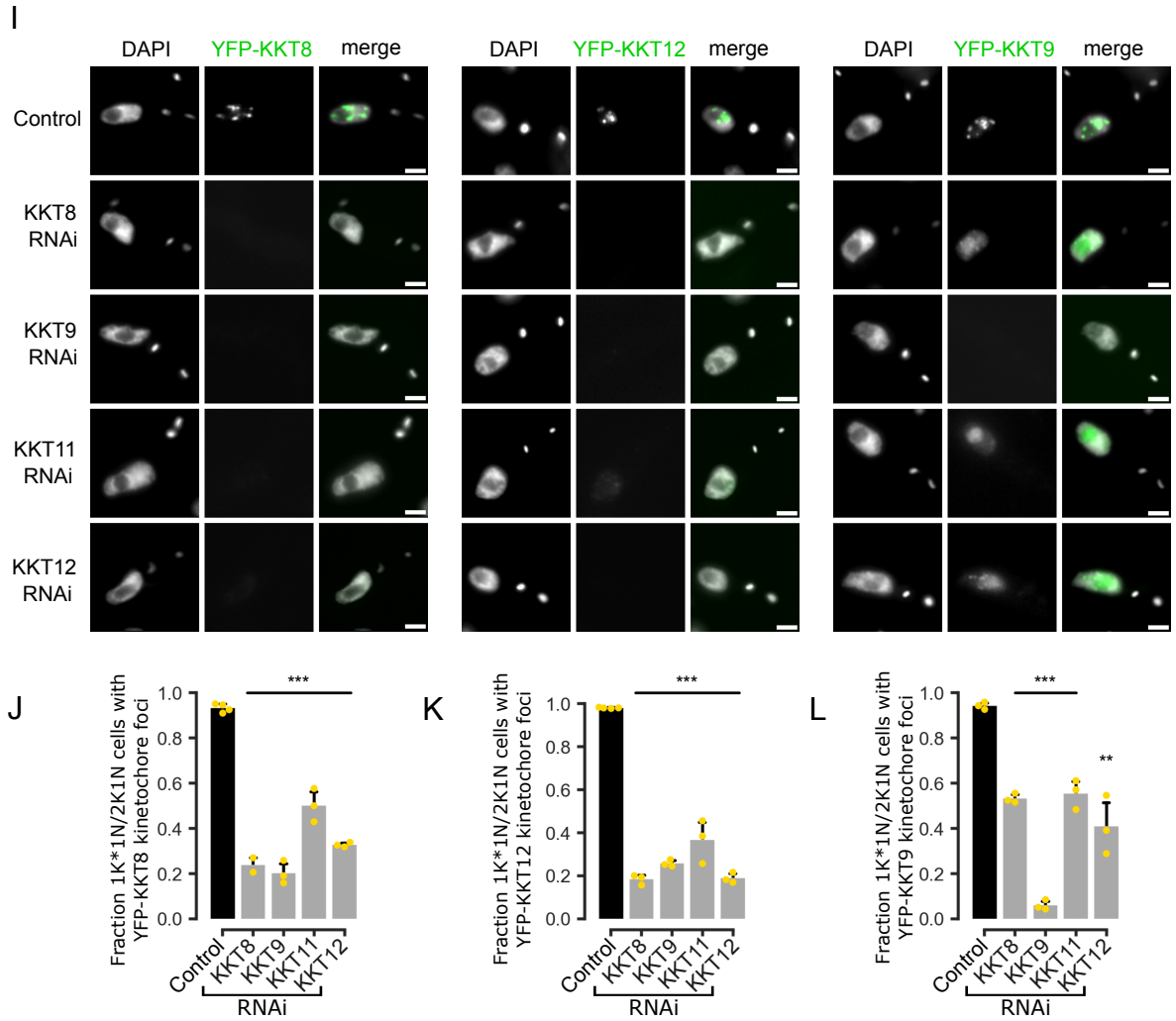
I
DAPI
YFP-KKT8
merge
DAPI
YFP-KKT12
merge
DAPI
YFP-KKT9
merge
Control
KKT8 RNAi
KKT9 RNAi
KKT11 RNAi
KKT12 RNAi
J
Fraction 1K*1N/2K1N cells with YFP-KKT8 kinetochore foci
***
Control
KKT8
KKT9
KKT11
KKT12
RNAi
K
Fraction 1K*1N/2K1N cells with YFP-KKT12 kinetochore foci
***
L
Fraction 1K*1N/2K1N cells with YFP-KKT9 kinetochore foci
***
**

A

Figure S5 (1)

T. brucei
T. congolense
T. cruzi
T. grayi
T. theileri
T. vivax
L. mexicana
Endotrypanonum
Leptomonas
Crithidia
Blechomonas
Phytomonas
B. saltans
P. confusum
A. hoyamushi
N. designis
A. spirali
P. ankaliazontas
Perkinsela

Figure S5 (ii)

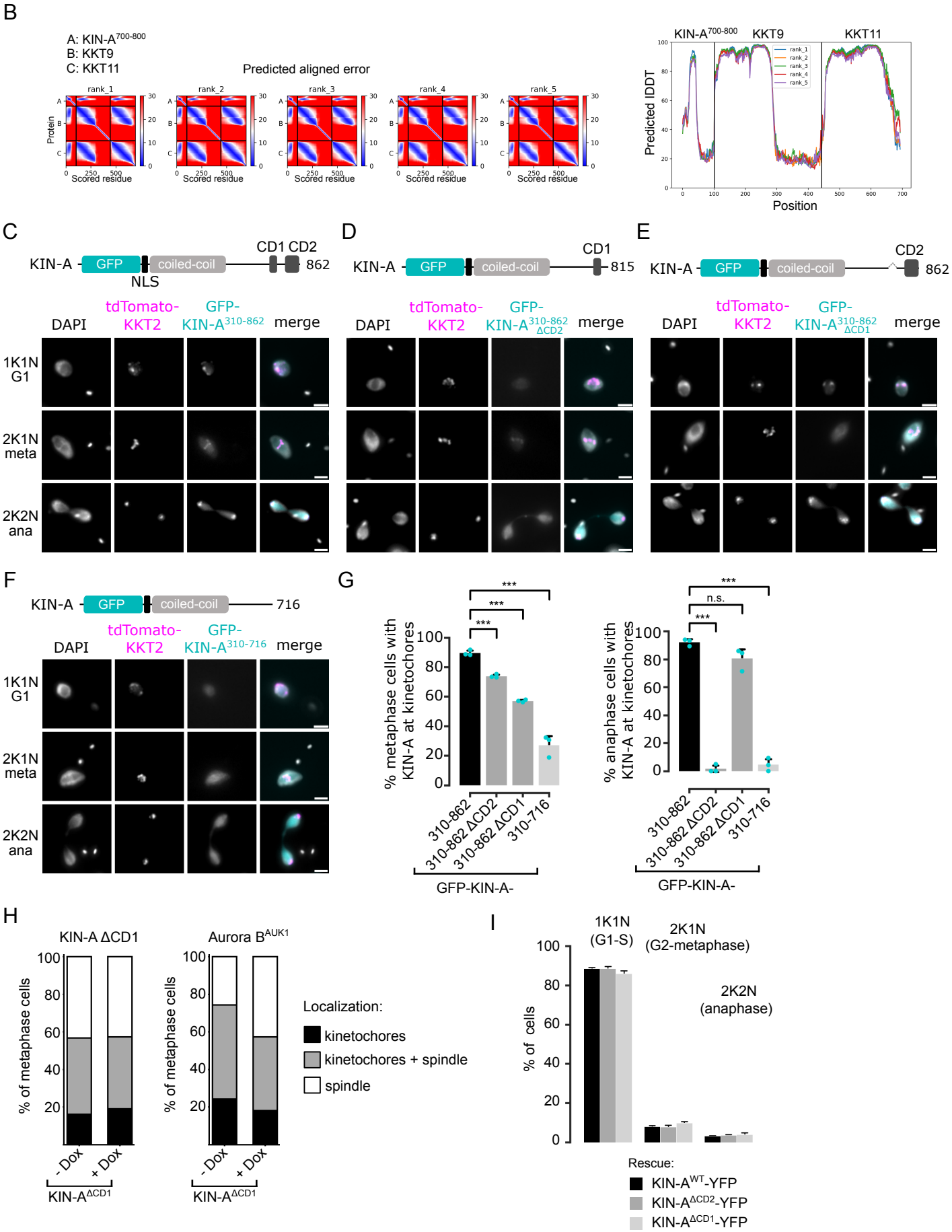
B
A: KIN-A700-800
B: KKT9
C: KKT11
Predicted aligned error
rank_1
rank_2
rank_3
rank_4
rank_5
Protein
Scored residue
KIN-A700-800
KKT9
KKT11
Predicted lDDT
Position
C
KIN-A
GFP
coiled-coil
NLS
CD1 CD2
862
DAPI
tdTomato-KKT2
GFP-KIN-A310-862
merge
1K1N G1
2K1N meta
2K2N ana
D
KIN-A
GFP
coiled-coil
CD1
815
GFP-KIN-A310-862 ΔCD2
E
KIN-A
GFP
coiled-coil
CD2
862
GFP-KIN-A310-862 ΔCD1
F
KIN-A
GFP
coiled-coil
716
GFP-KIN-A310-716
G
% metaphase cells with KIN-A at kinetochores
% anaphase cells with KIN-A at kinetochores
***
n.s.
310-862
310-862 ΔCD2
310-862 ΔCD1
310-716
GFP-KIN-A-
H
KIN-A ΔCD1
Aurora BAUK1
% of metaphase cells
- Dox
+ Dox
KIN-AΔCD1
Localization:
kinetochores
kinetochores + spindle
spindle
I
1K1N (G1-S)
2K1N (G2-metaphase)
2K2N (anaphase)
% of cells
Rescue:
KIN-AWT-YFP
KIN-AΔCD2-YFP
KIN-AΔCD1-YFP

A

Figure S6 (i)

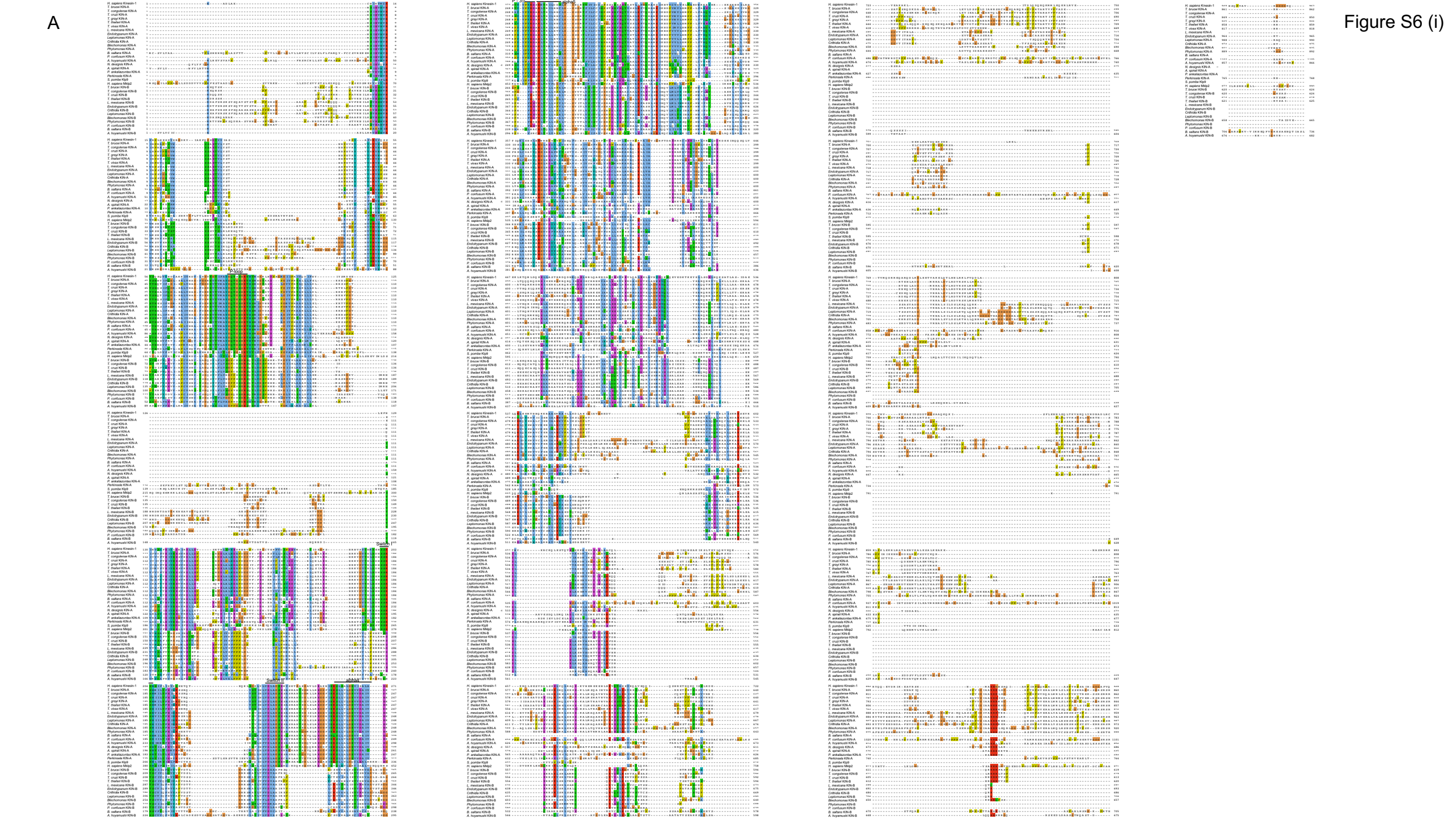

Figure S6 (ii)

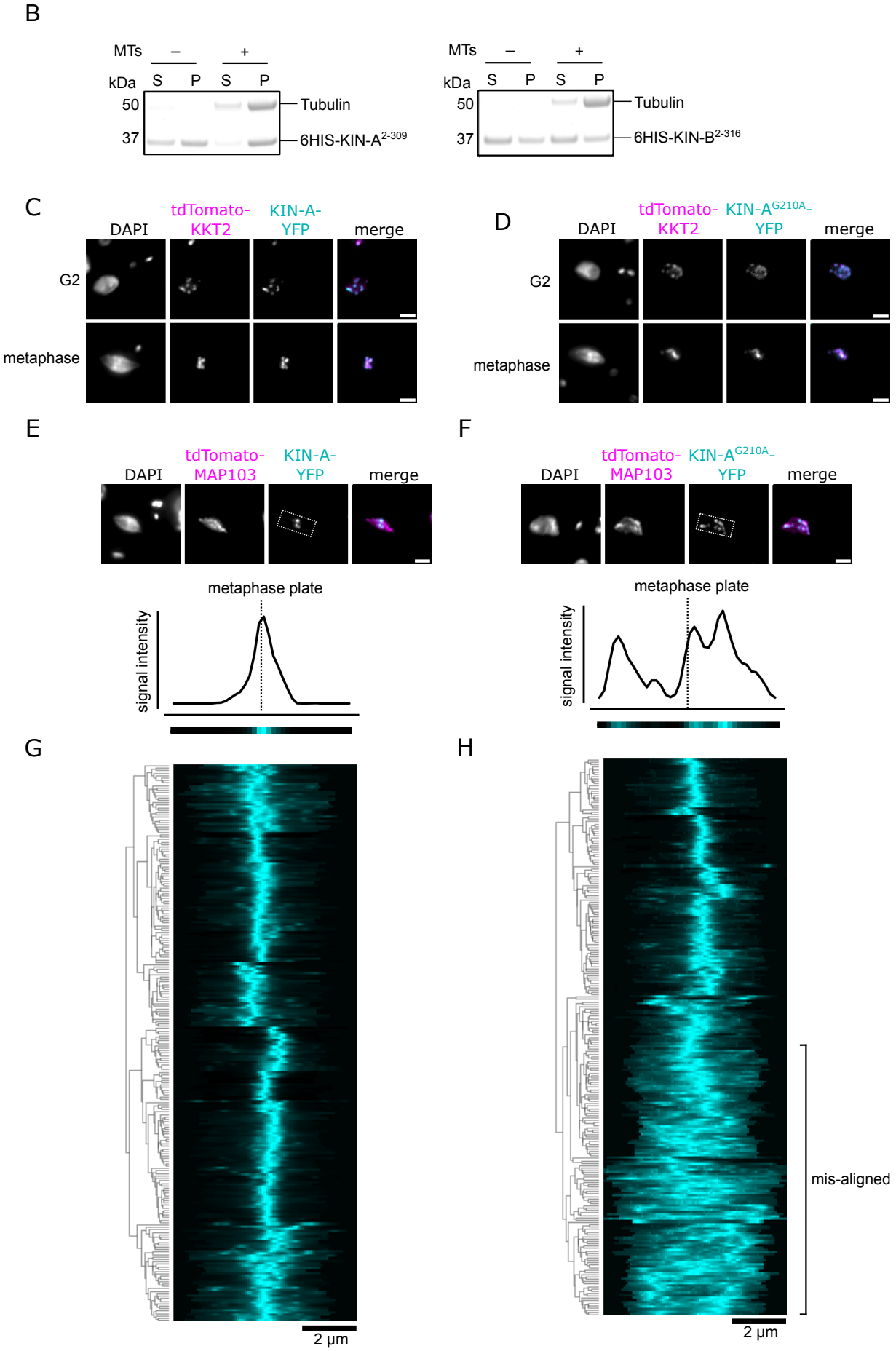
B
MTs
–
+
kDa
S
P
S
P
50
37
Tubulin
6HIS-KIN-A2-309
6HIS-KIN-B2-316
C
DAPI
tdTomato-KKT2
KIN-A-YFP
merge
G2
metaphase
D
KIN-AG210A-YFP
E
tdTomato-MAP103
F
metaphase plate
signal intensity
G
H
2 µm
mis-aligned